A new lunar high-Ti basalt type defined from clasts in Apollo 16 breccia 60639

A.L. Fagan [a,b,c,*], C.R. Neal [a,b]

[a] Department of Civil and Environmental Engineering and Earth Sciences, University of Notre Dame, Notre Dame, IN 46556, United States
[b] NASA Lunar Science Institute, United States
[c] Geosciences and Natural Resources Department, College of Arts and Sciences, 331 Stillwell Building, Western Carolina University, Cullowhee, NC 28723, United States

Abstract

This paper reports the detailed examination of three basalt clasts from Apollo 16 breccia 60639 that represent a new variant of high-Ti basalt returned from the Moon by the Apollo 16 mission. Mineral chemistry and whole-rock analyses were conducted on aliquots from three clasts (breccia matrix, basalt, and basalt + breccia matrix). The basalt clasts, which are not overtly porphyritic, contain compositionally zoned pyroxene, olivine, and plagioclase crystals that represent the evolution of the magma during crystallization; ilmenite does not exhibit major-element compositional zoning within individual crystals. Mineral compositions are distinct between the basalt and breccia matrix lithologies. In addition, whole-rock analyses identify clear compositional differences between the basalt and breccia matrix lithologies in both major and trace element concentrations. The composition of the mixed lithology aliquots (i.e., basalt + breccia matrix) do not indicate simple two component mixing (i.e., compositions are not intermediate to the basalt and breccia end-members); this apparent incongruity can be accounted for by adding ~19–40% plagioclase to an amalgamation of the average basalt and individual breccia clast compositions via impact mixing. Whole-rock analyses are consistent with previous analyses of one 60639 basalt clast, which were interpreted to indicate chemical similarity with Apollo 11 and 17 basalts. However, both major and trace elements suggest that the 60639 basalt clasts examined here have compositions that are distinct from Apollo 11 and 17 high-Ti basalts. Although the 60639 basalt clasts have similar characteristics to a variety of previously identified basalt types, the more extensive whole-rock analyses reported here indicate that they represent a type of Apollo high-Ti basalt heretofore unrecognized in the Apollo and lunar meteorite collections. By placing these new analyses in the context of other mare basalt compositions, a petrogenetic model for the basalts found in breccia 60639 is presented.

1. INTRODUCTION

The Apollo landing sites were predominantly located in mare areas, with the exception of Apollo 16, which landed in the Descartes highlands region. The Apollo 16 area is dominated by highlands anorthositic material and appeared to be devoid of mare deposits. Rare basaltic samples and glasses are, however, present (Table 1) as fragments in regolith samples or as small clasts in breccias, as with breccia 60639 (e.g., Dowty et al., 1974; Delano, 1975; Murali et al., 1976; Ma et al., 1976; Simon and Papike, 1987; Zeigler et al., 2006). It was assumed that these samples were introduced to the Descartes Highlands from elsewhere on the Moon as impact ejecta given the lack of visible local mare deposits.

* Corresponding author at: Geosciences and Natural Resources Department, College of Arts and Sciences, 331 Stillwell Building, Western Carolina University, Cullowhee, NC 28723, United States.
E-mail address: alfagan@wcu.edu (A.L. Fagan).

Table 1
Compositions of previously examined basalts from the Apollo 16 site.

Sample	60503,22–7	60603,10–16	62243,10–22	65703,9–13	60053,2–9	60639	60639,4	60639,5	60255
Basalt type	HT	HT	VLT	VLT	HA	HT	HT	HT	LT
Reference	Zeigler et al. (2006)	Zeigler et al. (2006)	Zeigler et al. (2006)	Zeigler et al. (2006)	Zeigler et al. (2006)	Dowty et al. (1974)	Murali et al. (1976)	Murali et al. (1976)	Simon and Papike (1987)
Major and Minor element oxide concentrations (wt%)									
SiO_2	41.8	34.8	46.4		47.1	44.8	42	41	47.98
TiO_2	8.7	14.5	0.8	0.5	2.0	6.3	7.9	6.8	1.58
Al_2O_3	9.9	5.5	11.9		15.4	15.1	12.4	12.4	10.82
Cr_2O_3	0.49	0.83	0.55		0.06	0.15	0.288	0.312	0.46
FeO	18.4	23.0	18.6	21.4	18.0	16	20.1	19.9	17.00
MnO	0.27	0.24	0.29		0.27	<0.01	0.255	0.249	0.28
MgO	10.5	13.0	10.1		3.4	5.2	5.5	7.5	9.00
CaO	10.1	6.9	10.8	12.1	13.4	11.5	10.6	10.7	12.49
Na_2O	0.30	0.46	0.2	0.218	0.35	0.68	0.563	0.592	0.27
K_2O	0.02	0.17	<0.02		0.03	0.15	0.13	0.14	0.01
P_2O_5	n.a.	0.07	0.04		n.a.	0.12			
Mg#	50.4	50.2	49.2		25.2	36.7	32.8	40.2	48.5
Trace element concentrations (ppm)									
Sc	74.4	46	59.8	56.4	60.3		75	71	
V							79	76	
Cr	3750	6160	3830	2150	900				
Co	43.4	57.4	30.1	21.6	20.8		19	21	
Ni	130	<130	110	<190	<190				
Sr	130	240	<200	<200	<240				
Zr	150	380	<160	<250	<500				
Ba	<90	222	<50	<30	97		180	160	
La	3.85	14.46	1.97	1.19	4.7		15	16	
Ce	11.9	39.6	5.6	3.9	13				
Nd	<24	35	<14	<30	9				
Sm	5.47	11.35	1.338	1.098	3.54		13.7	14.7	
Eu	1.14	2.56	0.39	0.47	1.02		2.91	2.95	
Tb	1.55	2.38	0.34	0.32	0.91				
Dy							20	20	
Yb	5.93	5.79	1.84	1.9	5.17		12.1	12.0	
Lu	0.9	0.775	0.282	0.282	0.763		1.8	1.9	
Hf	5.14	11.05	0.96	0.84	2.79				
Ta	0.94	2.61	0.11	<0.3	0.25				
Ir (ppb)	<15	<6	<10	<4	<5				
Au (ppb)	<12	<7	<8	<3	<3		14	19	
Th	0.21	1.55	0.12	0.07	0.41				
U	<0.7	0.45	<0.5	<0.17	0.21				

HT: High-Ti basalt, VLT: Very Low-Ti basalt, HA: High-Al basalt, LT: Low-Ti basalt; n.a.: not analyzed. Elements that are not reported are left blank.

Basaltic samples from Apollo 16 exhibit a fairly wide compositional range (cf., Zeigler et al., 2006), particularly with respect to the Ti concentration (0.5–14.5 wt% TiO$_2$, Table 1). Delano (1975) examined six crystalline basalt samples of varying sizes (∼100 µm to 7 mm) from Apollo 16: 66043,2,17 (high-Ti basalt); 61501 (high-Ti basalt fragment); 60003,230 (high-Ti basalt fragment); 60003,246 (fragment similar to Apollo 12 Ilmenite basalts); 60003,248 (high-Al/low-Ti basalt fragment); and 60003,250 (low-Ti basalt fragment). Simon and Papike (1987) examined a basalt clast from regolith breccia 60255 and found evidence of shock and possible reheating (presence of pyroxene exsolution lamellae). A calculated bulk composition based on mineral compositions and modal mineralogy suggested that the clast is a low-Ti basalt similar to the Apollo 15 quartz-normative (pigeonite) basalts. Hughes and Schmitt (1988) later confirmed that 60255 is a low-Ti basalt based on the composition of two chips (4.6 and 9.8 mg) extracted from the original clast 60255,21. The 60255 basalt clast has lower Th, Light Rare-Earth Elements (LREE), Hf, and Ta concentrations than low-Ti basalts from Apollo 12 and 15, but has higher Yb, Lu, and Sc concentrations (Hughes and Schmitt, 1988).

In contrast to these basalts, Garrison and Taylor (1980) analyzed the composition of a low-K Fra Mauro-type basalt clast (LKFM) in the highland breccia 66095, and suggested that a component of KREEP (i.e., composition rich in K, P, and REE) was present at the Apollo 16 site. Most recently, Zeigler et al. (2006) examined the chemical composition of five mare basalt fragments from the Apollo 16 coarse-fines size fraction (2–4 mm), which exhibited variable compositions (discussed in detail in Section 5.3). In addition to the chemical characterization, Zeigler et al. (2006) employed Clementine remote sensing data to constrain probable origins of the exotic basalt fragments (i.e., from Mare Tranquillitatis, Mare Nectaris/Sinus Asperitatis, Mare Vaporum).

The basalts from Apollo 16 reported here were found as clasts in breccia sample 60639 (original mass 175.1 g), which is a polymict fragmental breccia rake sample, collected near the Apollo 16 Lunar Module (LM). The sample contains a variety of lithic clasts including mare basalt and anorthosite, as well as poikilitic, aphanitic, and glassy impact-melt breccias (Ryder and Norman, 1980). A basalt clast from 60639 was first examined by Dowty et al. (1974), who posited that it was chemically similar to subophitic Luna 16 basalts based on broad-beam electron microprobe analysis. Delano (1975) included this basalt clast (60639,1) in his larger study of Apollo 16 mare-derived rocks and glasses and agreed with the conclusion of Dowty et al. (1974). Subsequent studies (Murali et al., 1976; Ma et al., 1976) suggested that the major- and trace-element concentrations in the 60639,1 basalt clast were similar to low alkali Apollo 11 and 17 high-Ti basalts. Given the geologic context of the Apollo 16 mission, whose prime objective was to sample highlands material (cf., Hinners, 1972), any basalt fragment can be considered exotic and thus is of particular interest, as it may represent a basalt type that has not been previously sampled and from a location hitherto unexamined.

The purpose of this study is to characterize two recently discovered basalt clasts from Apollo 16 breccia 60639, as

well as to re-examine the previously studied basalt clast (Dowty et al., 1974; Delano, 1975; Murali et al., 1976; Ma et al., 1976) with newer analytical techniques. New mineral and whole-rock data augment the sparse petrographic dataset for basalts from the Apollo 16 landing site (cf., Delano, 1975; Zeigler et al., 2006) and directly address the call to quantify the variability of lunar basalts set forth by the National Research Council Report (2007). The breccia matrix was also analyzed to determine if some of the basalt sample aliquots were actually mixtures of basalt and matrix. We examine major and trace element compositions of mineral phases in the previously studied thin-section 60639,2, which is the same sample examined by Dowty et al. (1974) and originates from Clast 1 (Table 2; Fig. 1). We also examine two thin-sections made from two "new" clasts discovered during a visit to the Curatorial Facility at Johnson Space Center and referred to here as

Table 2
Identification of lithologies present in each 60639 aliquot.

60639 subsamples	Lithologies present	Aliquot type	Parent Clast
,1	B	WR	1
,2	B, X	TS	1
,4	B	WR	1
,44	B, M	WR (2)	2
,45	B, X, M	WR (3)	2
,48	B, X, M	WR (3)	3
,50	B, X	TS	3
,52	B, X	TS	2

The subsample aliquot type is characterized as WR = whole-rock and TS = thin-section. The number listed in parentheses next to WR indicates the number of lithologies present and subsequent number of WR samples analyzed. B-basalt, X-breccia, M-mixture. Parent Clast 1 was discovered in the 1970s, while Clasts 2 and 3 were discovered in 2010.
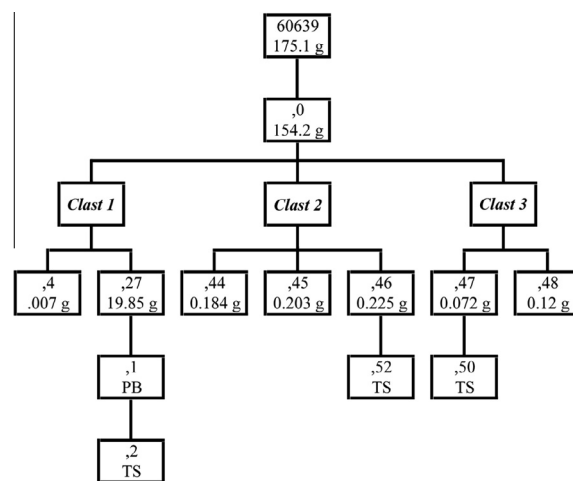

Fig. 1. Family tree lineage of each subsample of 60639 used in this study (see Table 1) including petrographic thin-sections (TS) and whole-rock aliquots (weight indicated in grams); PB indicates a potted butt.

Clasts 2 and 3 (Table 2; Fig. 1). The new data are put in the context of other lunar basalt compositions and a petrogenetic model is developed for the 60639 basalt clasts.

2. GEOLOGIC CONTEXT AND SAMPLE DESCRIPTION

Sample 60639 was collected during Extra-Vehicular Activity 3 of the Apollo 16 mission at station 10′, which was also known as the general location of the Lunar Module (LM) and Apollo Lunar Surface Experiments Package (ALSEP). Station 10′ lies approximately 70 m W-SW of the LM in a region with approximately level terrain, no craters in the immediate vicinity, and with ∼1/8 of the collected rocks having been buried in the regolith (Sutton, 1981). The top portion of 60639 is completely coated in glass (Morris et al., 1986), but the remaining sides are free of such a coating. The newly discovered basalt clasts once resided on the bottom side of 60639 in close proximity to an anorthosite fragment (Warren and Wasson, 1978).

The Clast 1 basalt aliquot (60639,2; Fig. 2) is a coarse-grained, subophitic, feldspathic mare basalt (Delano, 1975; erroneously quoted this thin section as being 60639,1). The petrographic thin-section contains the basalt clast in direct contact with a breccia matrix. The new thin-sections (,50 from Clast 3 and ,52 from Clast 2) are petrographically similar to Clast 1 (Fig. 2), which was extensively described by Delano (1975). Descriptions of the 60639 basalt clasts in this paper pertain directly to subsample 60639,2, but can be extrapolated to embrace the new samples in an effort to avoid repetitive petrographic descriptions. The modal mineralogy is approximately 50% pyroxene, 35% plagioclase, 5–10% ilmenite, 5–10% olivine, and accessory chromite-ulvöspinel phases (Delano, 1975), which is illustrated in the composite false-color X-ray map of Mg, Al, and Si (Fig. 3). Pyroxene crystals (∼150–675 μm) are subhedral with at least one identified crystal having a pyroxferroite composition (Delano, 1975). Two types of plagioclase have been identified: subhedral to euhedral blocky crystals (∼250–650 μm in length) and laths (∼200–450 μm). Ilmenite crystals (150 to 1 mm) are generally lath-like, but also occur as subhedral, blocky grains. Olivine crystals (∼150–420 μm) are anhedral to subhedral

and, in some cases, display ragged edges that Delano (1975) suggested were due to reaction with the residual liquid during crystallization. Chromite-ulvöspinel inclusions are present in a few olivine crystals and Delano (1975) identified ulvöspinel in some pyroxene crystals. The petrography indicates the presence of minor metallic phases in the mesostasis regions of the basalt clasts, but metal is more prevalent in the breccia portion of the thin-section. The mesostasis is Si-rich (Fig. 3), and contains minor sulfide and phosphate phases. Delano (1975) determined the crystallization sequence of major phases in the 60639,2 basalt as early saturation of plagioclase + Al-chromite + olivine → Cr-ulvöspinel → ilmenite → pyroxene, which is consistent with the whole-rock composition (see below).

The new basalt clasts are petrographically similar to Clast 1. In addition to mineral analyses, the whole-rock (WR) composition of five basalt subsamples (two from Clast 1; two from Clast 2; one from Clast 3) as well as three breccia subsamples (one from Clast 2; two from Clast 3) and two basalt + breccia matrix mixed lithology subsamples (both from Clast 2) from 60639 were analyzed (Table 2). WR split 60639,4 (Clast 1) derives from the same clast studied by Murali et al. (1976) and Ma et al. (1976).

Crystals in the breccia portion of 60639,2 exhibit significantly different morphologies from their basaltic counterparts (Figs. 2 and 3). The most noticeable difference between the two lithologies is the complete lack of ilmenite in the breccia as well as the higher concentration of metallic iron (up to 440 μm in the largest dimension, Fig. 3a and c); metal particles in the breccia contain 6 to 9 wt% Ni, but particles within the basalt were too small to analyze. The dominant mineral species within the breccia matrix is plagioclase, which range in size from ∼90 μm to >1 mm, but lath-like plagioclase crystals are conspicuously absent.

3. ANALYTICAL APPROACH

3.1. Mineral chemistry

Chemical compositions of mineral phases were determined for both the breccia and basalt portions in the three thin-sections (Table 2). Major and minor element mineral analyses were conducted on each thin-section; only
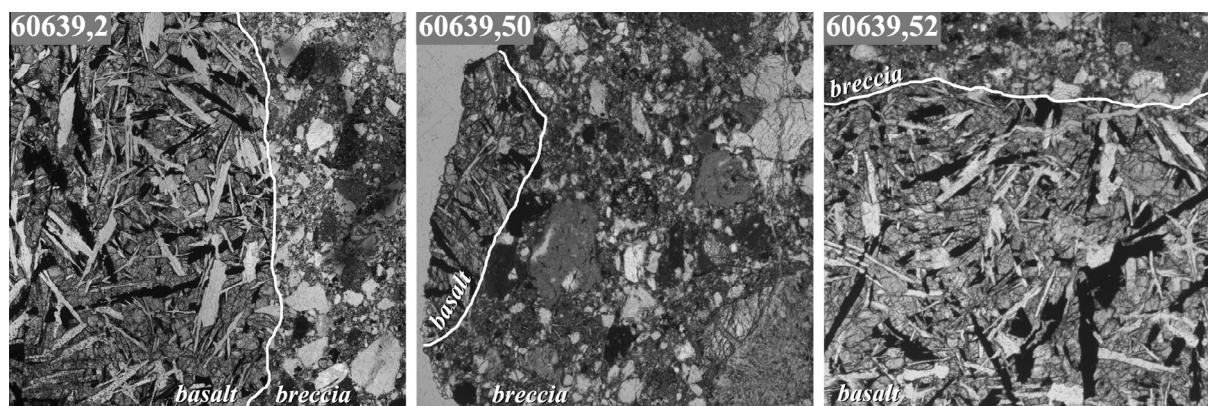

Fig. 2. Representative photomicrographs of petrographic thin sections ,2 (Clast 1); ,50 (Clast 3); and, 52 (Clast 2) of 60639 basalt fragments. Each basalt clast is in contact with a breccia matrix as indicated by a white line dividing the two lithologies. Field of view for each sample is 3 mm.
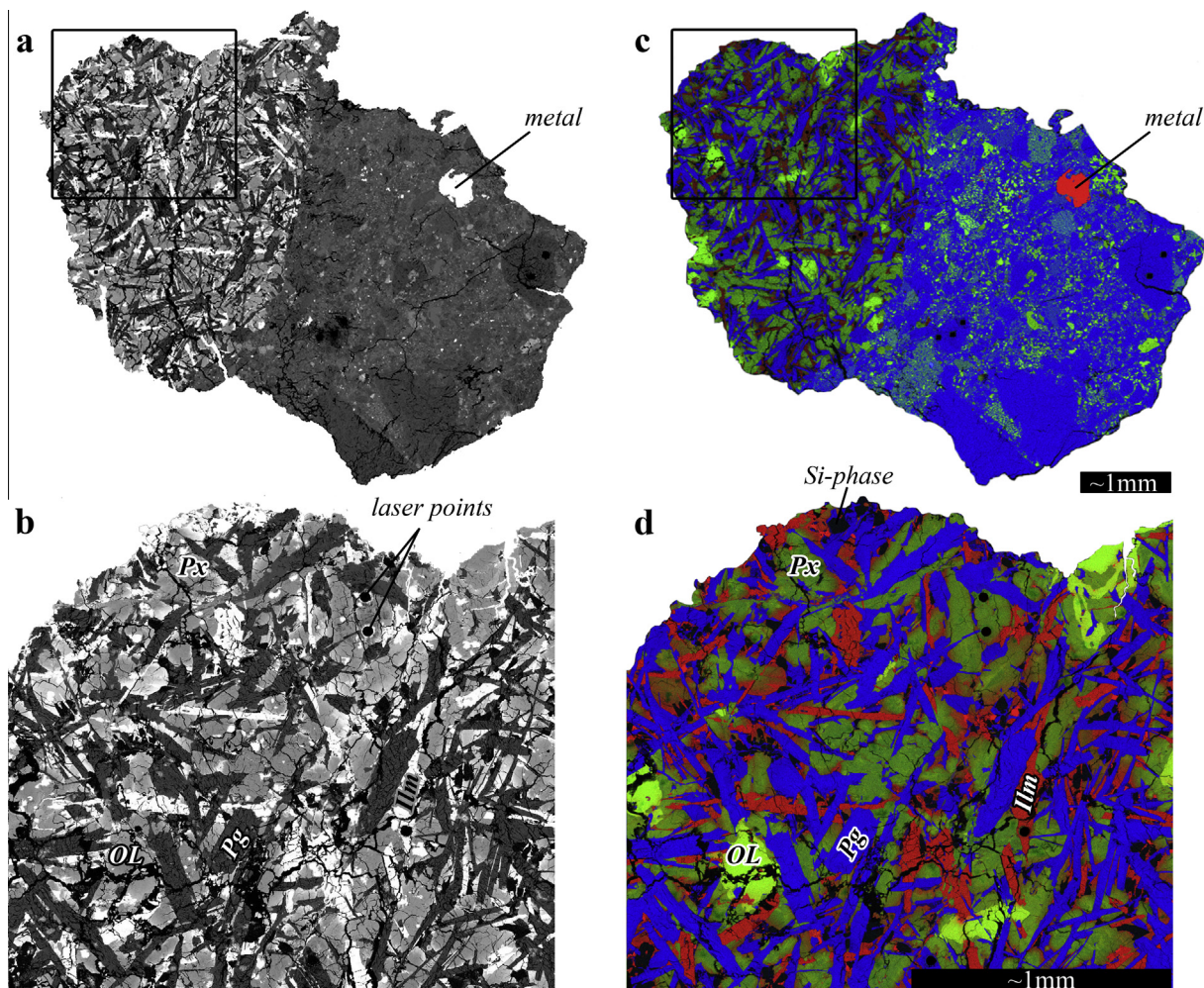
Fig. 3. Back-Scatter Electron (a and b) and X-ray composite (c and d) maps of a portion of thin-section 60639,2. Maps in (b) and (d) are enlarged portions of the boxes in (a) and (c) showing the different mineral phases present in the basalt clasts. The X-ray composite shows Fe as red, Mg as green, and Al as blue. Examples of the mineral phases are labeled: Px = pyroxene, OL = olivine, Pg = plagioclase, Ilm = ilmenite.

60639,2 was subjected to highly selective trace element analyses in an effort to retain as much of these precious samples as possible, while examining the correlation between major and trace element zoning in the different mineral phases. Major and minor element mineral analyses, as well as the collection of X-ray maps, were conducted using a JEOL JXA-8200 electron microprobe at the Washington University (St. Louis) Earth and Planetary Sciences Microanalysis Facility. All analyses used a 15 kV accelerating potential, 25 nA beam current, 5-μm spot size, and 30 s on-peak counting time. The instrument was calibrated using both natural and synthetic mineral standards. Detection limits ranged 0.02–0.06 wt% (2σ). Data were reduced using *Probe for EPMA* software and are reported in Tables EA1-EA7 within the Electronic Annex.

Trace element data were collected using laser ablation-inductively coupled plasma-mass spectrometry (LA-ICP-MS) using a New Wave UP-213 laser ablation system with He carrier gas coupled with a ThermoFinnigan Element2 ICP-MS at the University of Notre Dame's Midwest Isotope and Trace Element Research Analytical Center

(MITERAC). Concentrations obtained by electron-probe microanalysis (EPMA) were used as the internal standards for trace element analyses using LA-ICP-MS; internal and external standards were dependent on the mineral phase. Calcium concentrations, determine by EPMA, were used as the internal standard for plagioclase and pyroxene analyses; similarly, Ti and Mn were used as the internal standard for ilmenite and olivine analyses, respectively. Plagioclase and pyroxene analyses used the NIST SRM 612 glass as the external standard, whereas ilmenite and olivine used the NIST SRM 610 glass (Pearce et al., 1997). Measurements of the external standards were taken at the beginning and end of each analytical run. Analyses used a repetition rate of 5 Hz and corresponding fluence of ~16–18 J/cm^2. Laser spot size varied with crystal size and mineral phase: 15–25 μm for olivine, 40 μm for pyroxene, 40–65 μm for plagioclase, and 55 μm for ilmenite. For each individual analysis, the laser was warmed-up for ~20 s, background counts were collected for ~30 s, and the sample was ablated for ~60 s; the process was repeated following ~45 s of gas washout to ensure counts were back to

original background levels. Elemental concentrations were calculated using *GLITTER©* software (Van Achterbergh et al., 2001; XP version, Simon Jackson, Macquarie University) and are reported with uncertainties in Tables EA1-EA7 in the Electronic Annex.

3.2. Whole-rock chemistry

The basaltic clasts were plucked from 60639 by the curatorial staff at Johnson Space Center using stainless steel tools and the aliquots sent to the University of Notre Dame. All sides of each fragment were examined and photographed under the microscope to determine if the fragment was composed of (1) pure basalt, (2) breccia matrix, or (3) a mixed lithology of basalt + breccia matrix (Table 3). Where appropriate, aliquots were split into subsamples based on lithologic type as defined by: basalt, breccia, or a mixed lithology (basalt + breccia matrix). Some aliquots contained large amounts of breccia matrix that were unable to be successfully removed entirely from the basalt portions, thus these were classified as basalt + breccia mixtures. Two aliquots from Clast 1 (,1A and ,4; Table 3) were not subject to subdivision, as they were determined upon inspection to be composed entirely of basalt. Each aliquot and subdivision was hand-ground with an agate mortar and pestle in a Class 1000 clean laboratory; the mortar and pestle were cleaned with ultrapure (double distilled) HNO_3 (diluted to 5% with 18 MΩ H_2O) and thoroughly dried prior to use and between samples to avoid cross-contamination. Each sample was dissolved in ultrapure HF and HNO_3, in a ratio of 2:1, before being brought to a final volume of ∼100 g (∼10 g for smaller samples; i.e., aliquots ,4 and ,45; see Table 3) in 5% HNO_3. Dilution factors were noted and applied during data reduction. This dissolution does not allow Si to be directly measured, as dissolution in hydrofluoric acid forms volatile silica tetrafluoride, but it does allow all other major (and minor) elements to be quantified along with trace elements on the same sample aliquot. The SiO_2 concentration was calculated by difference. Given the low sample masses, this

method maximized the amount of data obtained for such small samples.

Major and minor element concentrations were quantified in solution-mode using a Perkin Elmer 3300 XL Optima ICP-Optical Emission Spectrometry (ICP-OES) at the University of Notre Dame's Center for Environmental Science and Technology (CEST). Instrument sensitivity was quantified using 6 calibration solutions of known concentrations, including a blank solution, and to the U.S. Geological Survey (USGS) basalt Standard Reference Material (SRM) BIR-1 (Flanagan, 1984; Gladney and Roelandts, 1988; Govindaruju, 1994). Three additional USGS SRMs (BHVO-1, BHVO-2, BCR-2) and two procedural blanks were also analyzed as unknowns ("unk"). Throughout the analyses, blanks (bk) and drift (D) correction samples were analyzed to follow instrument precision and drift in the analysis order of: D-unk-bk-unk-D-SRM-unk-bk-unk-repeat. Most aliquots and subsequent divisions were analyzed in triplicate for major element concentrations; exceptions were ,4-B (Clast 1) and ,45-B (Clast 2), which were only run in duplicate due to small sample sizes (Table 3). Each individual analysis represents an average of three consecutive measurements by the ICP-OES. This method for determining major elements in whole-rock samples via ICP-OES is described in more detail in Mahoney et al. (2001).

Trace element concentration data were collected via solution-mode ICP-MS with the Thermo-Finnigan Element2 ICP-MS instrument at MITERAC. The protocol of Neal (2001) was followed for analyses and data reduction (using the standard addition method). Procedural blanks and USGS SRMs were analyzed as unknowns. With the exception of the two smallest samples (,4-B and ,45-B), each sample was analyzed in duplicate. Some analyzed aliquots of the USGS SRMs had similar masses to the large (∼0.05 g) basalt clasts whereas others were similar to the smaller mass basalt clasts (∼0.003 g). Both sample sizes reproduced the reference data for these SRMs, which illustrates the representative nature of analyzing small masses. In addition, the relative homogeneity of the 60639 basalts suggests the small sample size did not introduce errors due to unrepresentative sampling.

3.3. Textural analysis

As a complement to compositional analyses, crystal size distributions (CSDs) can be used to quantitatively investigate igneous processes through the use of texture (e.g., Cashman and Marsh, 1988; Higgins, 1996). Plagioclase CSDs were determined for the basalt portion of Clasts 1 and 2 (thin sections ,2 and ,52). A CSD analysis was not performed on Clast 3 (,50) due to the small size of the basalt clast represented in the section (Fig. 2) and subsequent small population (<100) of plagioclase crystals; at least 250 crystals are deemed necessary to perform a statistically significant CSD analysis (Morgan and Jerram, 2006). Although pyroxene is more abundant in the basalt than plagioclase, the boundaries of the pyroxene grains are difficult to determine based on visual inspection of the thin section, thus plagioclase was selected as the preferred phase for

Table 3
Sample masses of aliquot subsamples used in determination of 60639 whole-rock chemistry.

60639 Subsample	Lithology in subsplit[*]	Mass (g)
,1A	B	0.057
,4	B	0.003
,44	B	0.048
	M	0.028
,45	B	0.002
	M	0.018
	X	0.055
,48	B	0.024
	M	0.035
	X	0.013

[*] Abbreviations for lithologies present in appropriate subsplits are as follows: B-basalt, X-breccia matrix, M-mixture of basalt and breccia matrix.

analyses. Furthermore, plagioclase CSDs can be directly compared to recent plagioclase CSDs from other Apollo basalts (Hui et al., 2011; Neal et al., 2015).

Individual plagioclase crystals were traced from digital photomicrographs using *Adobe Photoshop*® and imported into *ImageJ* (Higgins and Chandrasekharam, 2007), which can be used to measure the major and minor axes, roundness, and area of each crystal. Crystals with dimensions < 0.03 mm, approximately the thickness of the thin-section, are likely to be a projection of the crystal rather than an accurate measurement, thus crystals with the minor axis < 0.03 mm were eliminated so as not to skew the final dataset (Higgins, 2000). The major and minor axes of selected crystals were imported into *CSDslice* (Morgan and Jerram, 2006) to determine the best-fit short, intermediate, and long axes of the 3-D crystal habit. All determined crystal dimensions, habit, and total sample area were imported into *CSD corrections* 1.39 (Higgins, 2000, 2002; Higgins and Chandrasekharam, 2007), which calculates the 3-D CSD using 5 bins per decade. CSDs are traditionally represented as the natural log of the population density against the corrected crystal size length (Cashman and Marsh, 1988).

4. RESULTS

4.1. Mineral phase analyses

Individual mineral chemistries are reported in the Electronic Annex (Tables EA1-EA7) in order of the modal mineralogy of the 60639 basalt clasts (Delano, 1975); representative major- and minor-element mineral analyses are listed in Table 4. Pyroxene is the most abundant phase in the basalts (~50%) and is predominantly augite in composition, similar to Apollo 11 and 17 basalts (Fig. 4; Table EA1). Some pyroxene crystals are zoned with augite cores ranging to an Fe-rich rim. Pyroxene analyses from the basalt clasts reveal the presence of at least two Mg-rich and three Fe-rich pigeonite cores. The major element composition of pyroxenes, which are less common in the breccia, are generally similar between the different lithologies (Fig. 4a); an exception to this similarity is two enstatite grains ($Wo_{1.9-2.6}En_{51.9-55.4}Fs_{42.1-46.2}$) found in the breccia that is associated with Clast 3. Only pyroxenes from the Clast 1 basalt and Clast 3 breccia are Fe-rich.

Five trace element laser ablation analyses were conducted on pyroxene crystals from Clast 1 (Fig. 5; Table EA2). The pyroxene REE profiles are subparallel, but separate into two groups. The first group are less enriched in REE, have augite compositions, and form a tight cluster within Fig. 4a. The second group is more REE-enriched and includes the most Fe-rich augite (1-core) and an augite (3-core) that falls slightly outside of the clustered analyses.

Plagioclase, which constitutes approximately 35% of the 60639 basalt clasts (Delano, 1975), has distinct Anorthite (An) concentrations between the basalt and breccia lithologies (Fig. 6; Table EA3). All plagioclase from the breccia matrix are $>An_{97.1}$ (average $An_{97.9}$), whereas all plagioclase crystals from the basalt clasts are $<An_{95.2}$ (average $An_{93.5}$).

Major element compositions of plagioclase do not differ among the three basalt clasts. Four trace element analyses (Table EA4) were performed on 3 plagioclase grains: two crystals from the breccia and one (core and rim) from the basalt of Clast 1 (Fig. 6). Trace element data also distinguish between the basaltic and breccia plagioclase crystals with the basaltic crystal having higher Ti, Sr, and Eu concentrations (Table EA4).

The remaining phases compose the last 15% of the 60639 basalt clasts. Ilmenite crystals have an MgO range of 0.38–1.54 wt% with an average of 0.79 wt% (Table EA5). Major element concentrations of ilmenite do not appear to display any distinction between cores and rims, though the trace element chemistry may suggest minor variations in V, Zn, and Nb (Table EA6). Ilmenite is not found in the breccia matrix of the 60639 aliquots. Olivine crystals have an average Forsterite content of $Fo_{64.4}$ and $Fo_{69.1}$ from the basalt and breccia portions, respectively (Table EA7). A single olivine from the breccia matrix ("7-core" in Table EA7) was analyzed for trace elements and has similar Fo, Mn, and Co concentrations to the basaltic olivine crystals. However, the olivine from the breccia is distinct from the basaltic crystals, as it has lower concentrations of Sc (6.4 ppm), Ti (38 ppm), V (3.8 ppm), Cr (28 ppm), and Y (0.1 ppm) as well as being the only analyzed olivine with Ni above the detection limit. Basaltic olivine crystals that are the most enriched in Cr ($\geqslant$900 ppm) are also generally the most enriched in V (>35 ppm). Only one analyzed olivine has an Y concentration of >0.80 ppm; among the basaltic olivine, this olivine also has the lowest concentration of Ti (306 ppm), V (10.4 ppm), and Co (48), but the highest concentration of Mn (2924 ppm).

4.2. Whole-rock analyses

Despite small sample masses (<60 mg) for bulk composition determination, the compositions of the basalt aliquots are similar and variances may be explained by relative concentrations of particular phases within separate aliquots. Two basalt subsamples were each analyzed from Clast 1 and Clast 2, whereas only one basalt subsample was analyzed from Clast 3 (Tables 2 and 3). One breccia matrix subsample was analyzed from Clast 2 and one from 3 (Tables 2 and 3). Two mixed lithology subsamples (basalt + breccia matrix) were analyzed from Clast 2 and one from Clast 3 (Tables 2 and 3). No breccia matrix or mixed lithology subsamples were analyzed for bulk composition from Clast 1, as the WR aliquot was entirely composed of basalt. See Table 2 and Figs. 1 and 2 for the family lineage of each clast and representative photomicrographs.

Whole-rock major element chemistry (Table 5) can be used to distinguish between the basalt, the breccia matrix, and the mixed lithology (basalt + breccia matrix) (Fig. 7). Basalt samples have the highest concentrations of FeO, MgO, TiO_2, Cr_2O_3, and MnO. The breccia whole-rock analyses have the highest P_2O_5 concentration, whereas the basalt and mixed lithology analyses have similar P_2O_5 contents to each other. The Al_2O_3 concentrations (Fig. 7a) of the breccia and mixed lithology aliquots are similar to each other, but greater than those of the basalt, illustrating the

Table 4
Representative major- and minor-element mineral analyses from 60639 basalt aliquots.

Phase	Pyroxene						Plagioclase						Olivine				Ilmenite			
Subsample	,2		,50		,52		,2		,50		,52		,2		,50		,2		,52	
Crystal ID	3-core	±	1-rim	±	5-core	±	5-core	±	3-core1		3-core	±	5-core	±	1-core	±	5-core	±	1-core	±
Major and Minor element oxide concentrations (wt%)																				
SiO₂	50.2	0.10	49.3	0.09	48.4	0.09	45.0	0.09	46.8	0.09	45.6	0.09	37.4	0.08	38.2	0.09	N.A.		N.A.	
TiO₂	1.82	0.03	2.31	0.04	3.09	0.04	0.32	0.02	0.08	0.02	0.12	0.02	0.37	0.02	0.12	0.02	53.2	0.16	52.4	0.13
Al₂O₃	1.95	0.02	2.62	0.03	3.57	0.03	34.1	0.07	33.7	0.07	33.9	0.07	0.02	0.01	0.10	0.01	0.00	0.00	0.07	0.01
FeO	20.3	0.13	14.3	0.07	14.1	0.06	0.50	0.03	0.49	0.02	0.33	0.02	25.3	0.15	21.0	0.08	44.4	0.19	45.7	0.11
MnO	N.A.		0.26	0.02	0.31	0.02	0.04	0.02	0.00	0.01	0.03	0.01	0.26	0.02	0.26	0.02	0.42	0.03	N.A.	
MgO	10.3	0.05	12.6	0.05	13.9	0.06	0.20	0.01	0.22	0.01	0.24	0.01	35.6	0.09	39.8	0.09	1.54	0.02	0.52	0.02
CaO	16.1	0.06	17.2	0.06	15.2	0.06	18.0	0.06	17.1	0.06	17.8	0.06	0.30	0.01	0.24	0.01	0.05	0.01	N.A.	
Na₂O	0.03	0.01	0.07	0.01	0.06	0.01	1.10	0.02	1.33	0.02	1.22	0.02	n.d.		n.d.		0.02	0.02	N.A.	
K₂O	N.A.		0.00	0.01	n.d.		0.05	0.01	0.07	0.01	0.03	0.01	0.01	0.01	0.00	0.01	0.02	0.01	N.A.	
Cr₂O₃	0.27	0.01	0.39	0.02	0.57	0.02	N.A.		N.A.		N.A.		0.23	0.01	0.13	0.02	0.43	0.02	0.45	0.02
Total	100.7		99.1		99.2		99.2		99.8		99.2		99.5		99.8		100.1		99.2	
Cations per X oxygen atoms (X = 6 for Px, 8 for Plag, 4 for Olivine, 3 for Ilm)																				
Si	1.93		1.89		1.84		2.10		2.16		2.12		0.99		0.99		0.00		0.00	
Ti	0.05		0.07		0.09		0.01		0.00		0.00		0.01		0.00		1.00		1.00	
Al	0.09		0.12		0.16		1.87		1.83		1.85		0.00		0.00		0.00		0.00	
Fe	0.65		0.46		0.45		0.02		0.02		0.01		0.56		0.45		0.92		0.97	
Mn	0.00		0.01		0.01		0.00		0.00		0.00		0.01		0.01		0.01		0.00	
Mg	0.59		0.72		0.79		0.01		0.01		0.02		1.41		1.54		0.06		0.02	
Ca	0.66		0.71		0.62		0.90		0.85		0.88		0.01		0.01		0.00		0.00	
Na	0.00		0.01		0.00		0.10		0.12		0.11		0.00		0.00		0.00		0.00	
K	0.00		0.00		0.00		0.00		0.00		0.00		0.00		0.00		0.00		0.00	
Cr	0.01		0.01		0.02		0.00		0.00		0.00		0.00		0.00		0.01		0.01	
Total	3.97		3.98		3.98		5.01		4.99		5.00		3.00		3.00		2.00		2.00	
End-members: En	30.9		38.3		42.4		An 89.8		87.3		88.8		Fo 71.6		77.4					
Fs	34.3		24.3		24.1		Ab 9.92		12.3		11.0		Fa 28.4		22.6					
Wo	34.7		37.4		33.4		Or 0.27		0.40		0.20									
Mg#	47.4		61.2		63.7												5.81		2.00	

Elements not detected are denoted by n.d.
Elements not analyzed are denoted by N.A.
Pyroxene data are reduced on the basis of 6 oxygens and cation totals should sum to 4 – (Ca,Mg,Fe)₂Si₂O₆.
Plagioclase data are reduced on the basis of 8 oxygens and cation totals should sum to 5 – CaAl₂Si₂O₈.
Olivine data are reduced on the basis of 4 oxygens and cation totals should sum to 3 – (Mg,Fe)₂SiO₄.
Ilmenite data are reduced on the basis of 3 oxygens and cation totals should sum to 2 – FeTiO₃.
Criteria for a good analysis: oxide totals between 99 and 101 and cation totals ±0.05 of the ideal sum for the given mineral.
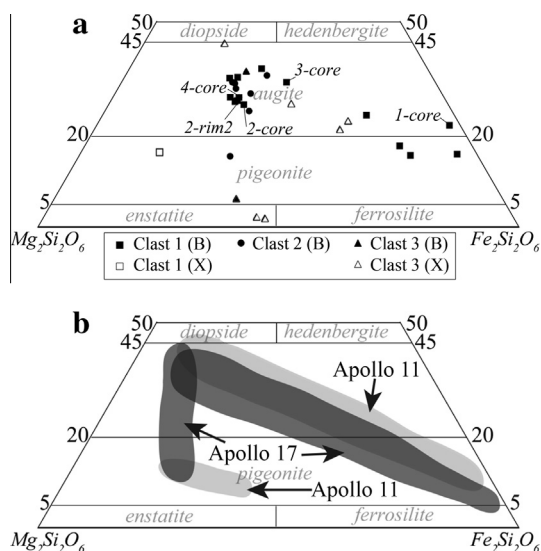
Fig. 4. Major element compositions of pyroxene from (a) 60639 basalt and breccia lithologies and (b) pyroxene compositional fields from Apollo 11 and 17 high-Ti basalts Papike et al. (1976).
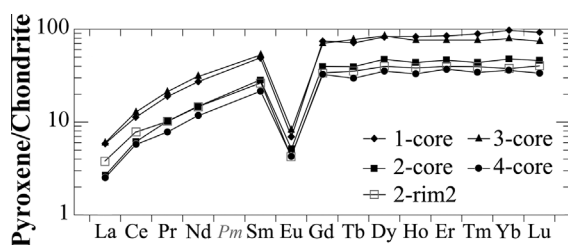

Fig. 5. REE compositions of selected basaltic pyroxene from 60639,2. The REE data are normalized to chondritic meteorites (Anders and Grevesse, 1989).

Fig. 6. Plagioclase major element (An% vs. TiO_2) compositions. Average error bars are shown and have been estimated from repeat analyses.

dominance of plagioclase in the breccia. All three lithologic types represented here have overlapping concentrations of CaO, K_2O, and Na_2O (Table 5).

The three analyzed lithologic groups are enriched in incompatible trace elements (Table 6, see Table 7 for USGS Standard Reference Materials) relative to chondrites (*cf.*, Anders and Grevesse, 1989; Fig. 7c). The basalt subsamples are enriched in Sc, V, Cr, Cu, Zn, Sr, Y, Zr, and Hf. The mixed lithology and breccia matrix subsamples exhibit higher concentrations of Ni and Co in response to the higher concentration of metal in the breccia (Table 6; Fig. 3). High-field strength elements also show a distinction between the groups: the basalt subsamples are the richest in Hf, Zr, Ta, and Y, but exhibit the lowest concentration of U and Th. In contrast, the breccia subsamples have the highest Th, whereas the mixed lithology subsamples generally exhibit low Zr, Hf, Y, and Ta but yield concentrations of Th and U that are intermediate to the basalt and breccia analyses. Among the large ion lithophile elements, the basalt subsamples have the highest concentration of Sr, but have the lowest Rb and Cs concentrations. In contrast, the breccia subsamples have the highest Rb and the mixed lithology subsamples have the lowest Ba; the mixed lithology and breccia subsamples have similar Cs and Sr concen-
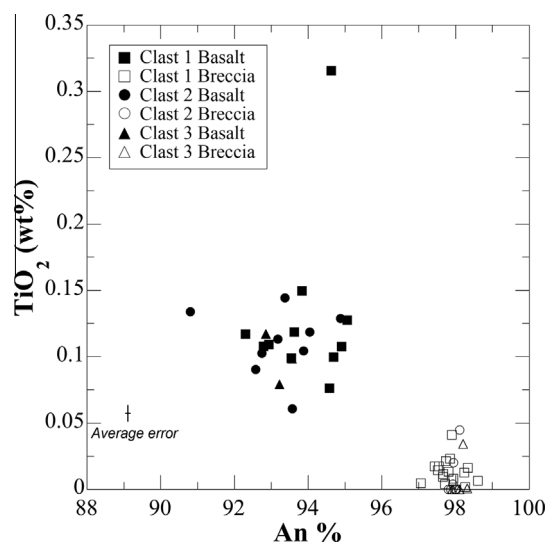
trations to each other. Finally, the breccia and mixed lithology subsamples are more enriched in Pb than the basalt subsamples by a factor of 2 to 4.

The REE profiles of the basalt clasts are subparallel and exhibit a slight concave down shape with a maximum in the middle REE (Fig. 7c). In contrast, both the breccia matrix and the mixed lithology subsamples display subparallel, LREE-enriched profiles and all exhibit a strong negative Eu anomaly. The Clast 3 breccia is enriched in the REE relative to the Clast 2 breccia, although the profiles are subparallel. Most notably, although the mixed lithology is a combination of basalt clast + breccia matrix, the REE profiles of these samples do not appear to reflect this association, as the mixed lithology subsamples do not display REE profiles purely intermediate to the basalt and breccia.

4.3. Crystal size distributions (CSD)

Plagioclase from the basalt portions of the Clasts 1 (,2) and 2 (,52) petrographic thin-sections have similar CSD profiles (Fig. 8a). Both CSDs are approximately linear and subparallel to each other. Clast 1 displays a downward curve at low crystal populations and Clast 2 appears to have a deficit of crystals in the ~0.3 mm size range. If, however, the Clast 2 CSD is extrapolated between the ~0.5 mm and the ~0.2 mm size bins, it is remarkably similar to that of Clast 1. The overall shapes of these plagioclase CSDs are similar to those from Apollo 14 high-Al Group B and C basalts (Fig. 8c and d), but not Group A basalts (Fig. 8b) (Hui et al., 2011; Neal et al., 2015).

5. INTERPRETATION AND DISCUSSION

5.1. Textural analyses

The linear nature of the basaltic plagioclase CSDs (Fig. 8) indicate uninterrupted crystal nucleation and

Table 5
60639 whole-rock major and minor element concentrations (wt%).

60639 subsample	,1		,4		,44		,44		,45		,45		,45		,48		,48		,48	
Lithology	B_{avg}		B_{avg}		B_{avg}		M_{avg}		B_{avg}		M_{avg}		X_{avg}		B_{avg}		M_{avg}		X_{avg}	
# Analyses	N = 3		N = 2		N = 3		N = 3		N = 2		N = 3		N = 3		N = 3		N = 3		N = 3	
Parent Clast[*]	1	±	1	±	2	±	2	±	2	±	2	±	2	±	3	±	3	±	3	±
Major and minor element oxide concentrations (wt%)																				
SiO_2[**]	43.1		40.3		42.2		43.5		40.9		43.8		48.0		41.9		44.8		43.1	
TiO_2	7.39	0.01	7.73	0.01	7.87	0.00	2.34	0.00	7.80	0.01	2.66	0.00	0.67	0.00	7.50	0.01	0.90	0.00	1.03	0.00
Al_2O_3	12.5	0.01	11.8	0.05	11.5	0.01	24.3	0.05	13.4	0.03	22.9	0.06	24.2	0.06	11.4	0.01	26.2	0.04	27.0	0.03
Cr_2O_3	0.24	0.00	0.24	0.00	0.28	0.00	0.13	0.00	0.19	0.00	0.13	0.00	0.11	0.00	0.33	0.00	0.10	0.00	0.10	0.00
FeO	17.8	0.02	19.4	0.03	19.0	0.04	7.92	0.01	18.3	0.01	8.55	0.01	5.43	0.01	19.1	0.01	5.41	0.01	5.73	0.01
MnO	0.25	0.00	0.28	0.00	0.26	0.06	0.10	0.00	0.25	0.00	0.12	0.00	0.06	0.00	0.26	0.00	0.07	0.00	0.07	0.00
MgO	6.58	0.00	7.13	0.00	7.38	0.06	6.03	0.02	*5.76*	*0.00*	6.67	0.02	6.64	0.01	8.14	0.02	6.36	0.02	6.03	0.01
CaO	11.2	0.01	12.4	0.02	10.6	1.47	14.9	0.01	12.7	0.01	14.4	0.01	13.9	0.02	10.6	0.01	15.3	0.02	16.1	0.02
Na_2O	0.55	0.00	0.48	0.00	0.53	0.01	0.46	0.00	0.55	0.00	0.43	0.00	0.48	0.00	0.48	0.00	0.48	0.00	0.43	0.00
K_2O	0.17	0.00	0.15	0.00	0.17	0.02	0.15	0.00	0.17	0.00	0.15	0.00	0.22	0.00	0.15	0.00	0.17	0.00	0.15	0.00
P_2O_5	*0.20*	*0.14*	*0.05*	*0.05*	*0.26*	*0.42*	*0.17*	*0.09*	n.d.	n.d.	*0.16*	*0.06*	*0.3*	*0.38*	*0.22*	*0.25*	*0.26*	*0.23*	*0.32*	*0.17*

Standard Reference Materials	BHVO-1		BHVO-2		BIR-1		BCR-2	
	Cert.	Avg (N = 2)	Cert.	Avg (N = 2)	Cert.	Avg (N = 2)	Cert.	(N = 1)
Major and minor element oxide concentrations (wt%)								
SiO_2[**]	49.9	50.2	49.9	50.1	48.0	47.7	54.1	54.9
TiO_2	2.71	2.74	2.73	2.71	0.96	0.97	2.26	2.26
Al_2O_3	13.8	13.7	13.5	13.8	15.5	15.7	13.5	13.6
Cr_2O_3	0.05	0.04	0.04	0.04	0.05	0.06	0.00	0.00
FeO	10.9	11.0	11.0	11.0	10.1	10.3	12.3	12.3
MnO	0.17	0.17	0.17	0.17	0.18	0.18	0.20	0.20
MgO	7.23	7.36	7.23	7.45	9.70	9.80	3.59	3.94
CaO	11.4	11.5	11.4	11.4	13.3	13.4	7.12	7.16
Na_2O	2.26	2.28	2.22	2.26	1.82	1.84	3.16	3.10
K_2O	0.52	0.63	0.52	0.62	0.03	0.03	1.79	2.10
P_2O_5	0.27	0.38	0.27	0.49	0.02	0.02	0.35	0.43

WR subsamples are identified by lithologic type such that B-basalt, X-breccia, and M-mixture of basalt and breccia. Analyses in italics are based on one analysis (arithmetic mean of 3 measurements). Elements not detected are denoted by n.d. One standard deviation is indicated in the columns denoted by ±.
Certified values for Standard Reference Materials (BHVO-1, BHVO-2, BIR-2, BCR-2) are from the United States Geological Survey (http://crustal.usgs.gov/geochemical_reference_standards/).
[*] Parent clasts are those represented in Table 1 and Fig. 1.
[**] SiO_2 is calculated by mass difference due to the hydrofluoric acid dissolution procedure, which volatilizes SiO_2.
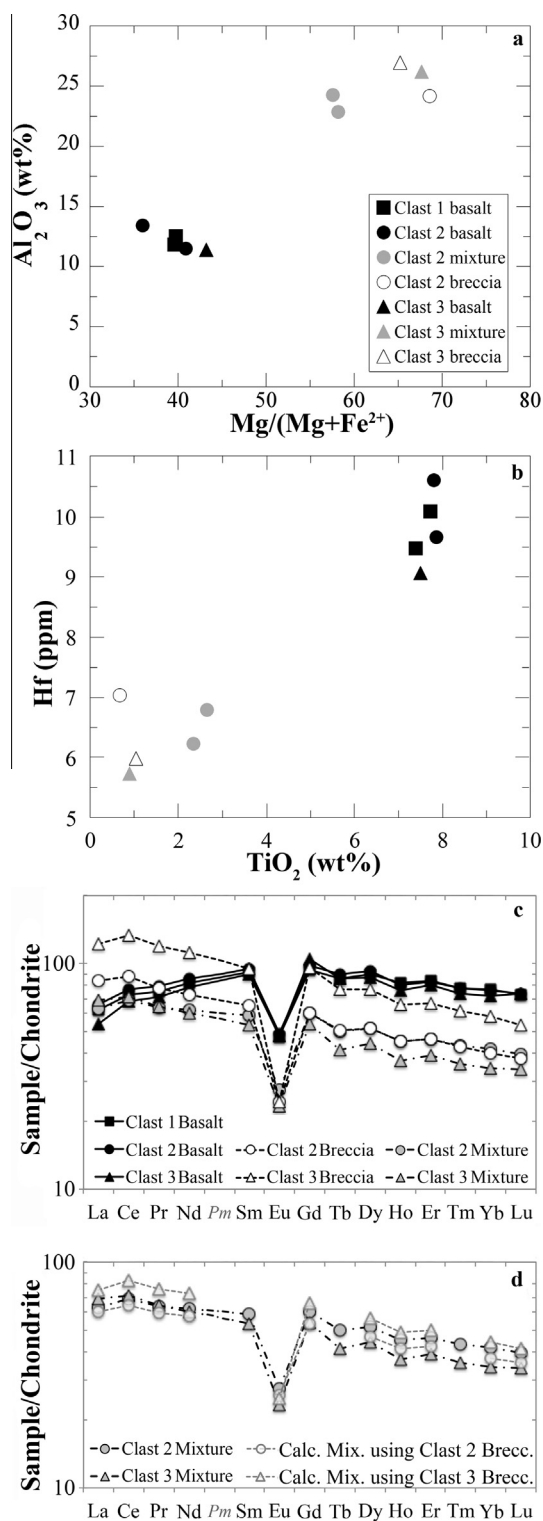
Fig. 7. Average whole-rock major element compositions of 60639 basalt, breccia matrix, and basalt + breccia mixed lithology: (a) $Mg/(Mg+Fe^{2+})$ vs. Al_2O_3 (wt%); (b) TiO_2 (wt%) vs. Hf (ppm); (c) average REE profiles normalized to chondritic meteorites (Anders and Grevesse, 1989); (d) Clast 2 and Clast 3 basalt + breccia mixed lithologies and mixing calculation REE profiles using the Clast 2 breccia and Clast 3 breccia from Table 8.

growth (Marsh, 1988, 1998) without substantial influence by crystal accumulation, magma mixing, or textural coarsening, which would alter the crystal nucleation and growth rates (e.g., Marsh, 1988; Higgins, 1996). This is consistent with the lack of plagioclase phenocrysts or any other phenocryst phase. The downward curve in Clast 1 at small corrected crystal lengths is likely a consequence of the resolution of the optical thin-section image used and number of crystals available. The total sample area and number of plagioclase crystals were larger for Clast 1 and the smaller crystal population of Clast 2 probably accounts for the slight downward kink at ∼0.3 mm (emphasized by a relatively large error on this data point). The similarity of the two plagioclase CSDs indicates the basalt clasts likely experienced similar cooling histories and may possibly have been derived from similar basalt flows (if not the same flow).

5.2. Mineral chemistry

All mineral phases are compositionally similar among the three basalt clasts and indicate that they probably represent fragments from the same basalt eruption if not the same flow unit. Plagioclase and pyroxene compositions reflect crystallization from an evolving magma through their core-to-rim zonations. For example, plagioclase rims generally have a higher Fe/(Fe + Mg) ratio than the cores (also reflected in the pyroxenes); plagioclase rims also have lower An contents due to increased Na_2O (Table EA3). These zonations are consistent with crystallization from an evolving melt. In addition, whereas the basaltic plagioclase typically display TiO_2 concentrations of 0.10 wt% or more, the breccia plagioclase crystals all have ⩽0.04 wt% TiO_2. The partition coefficient for Ti in plagioclase is substantially less than that in ilmenite, thus the composition of the basaltic plagioclase crystals confirm that they crystalized before ilmenite to produce high Ti concentrations; this crystallization sequence agrees with that suggested by Delano (1975). In contrast, the lower-Ti breccia plagioclase crystals likely crystallized from a different, lower-Ti melt.

Crystal chemistry of pyroxene shows that cores are generally enriched in Mg over Fe relative to the rims (Fig. 9a). At least one pyroxene (#2 in Clast 2) has a rim that is slightly more enriched in Mg over Fe relative to the core (Fig. 4a), which may indicate that the crystal was cut in such a way during the thin-sectioning process to cause the "rim" to more accurately reflect a core composition. The presence of Fe-rich pyroxene (Fig. 4a), including metastable pyroxferroite identified by Delano (1975), indicates rapid cooling (Lindsley et al., 1972). The pyroxene chemistry reported here is consistent with that determined by Delano (1975) and is also similar to pyroxene major element chemistry of mare-derived rocks from other Apollo 16 stations (Delano, 1975). Pyroxene analyses from the 60639 basalt clasts have Ti/Al ratios ∼0.5 (Fig. 9b) with cores typically more abundant in Ti and Al than the rims. Titanium and Al are incompatible in both Mg- and Fe-rich pyroxenes (Dygert et al., 2014), so a Ti/Al ratio of ∼0.5 is consistent with the original crystallization sequence

Table 6
60639 whole-rock trace element concentrations (ppm).

| 60639 Subsample | ,1-B_avg | | ,4-B | | ,44-B_avg | | ,44-M_avg | | ,45-B | | ,45-M_avg | | ,45-X_avg | | ,48-B_avg | | ,48-M_avg | | ,48-X_avg | |
| Parent Clast | 1 | | 1 | | 2 | | 2 | | 2 | | 2 | | 2 | | 3 | | 3 | | 3 | |
#	N:2	±	N:1	±	N:2	±	N:2	±	N:1	±	N:2	±	N:2	±	N:2	±	N:2	±	N:2	±
Li	10.5	0.13	14.7	0.23	10.5	0.07	8.38	0.22	14.4	0.24	8.24	0.33	9.38	0.35	7.34	0.14	9.39	0.30	4.55	0.16
Be	1.54	0.04	1.72	0.05	1.57	0.08	1.29	0.10	1.81	0.12	1.15	0.11	1.61	0.10	1.61	0.04	1.73	0.11	1.12	0.04
Sc	65.6	0.66	89.9	3.71	61.3	1.05	16.2	0.39	66.1	2.16	13.5	0.33	9.60	0.48	52.5	0.61	7.40	0.30	10.0	0.39
V	79.2	1.42	88.5	1.79	86.1	1.90	34.4	0.40	63.0	2.10	35.3	0.65	21.8	0.66	100	1.80	23.9	0.81	18.7	0.27
Cr	1803	20.9	1922	67.1	2130	49.3	982	10.9	1316	58.4	944	25.7	754	22.8	2553	24.4	747	26.2	577	13.4
Co	19.3	0.06	21.7	0.62	21.0	0.16	28.7	0.81	16.8	0.60	16.6	0.50	34.9	0.74	25.1	0.27	26.3	0.93	20.5	0.57
Ni	15.0	0.39	1.68	0.12	4.54	0.13	374	6.78	38.6	0.67	152	1.59	680	23.9	6.21	0.14	406	9.27	323	5.47
Cu	56.4	1.64	88.2	5.61	58.7	1.68	10.8	0.50	68.3	3.18	11.6	0.96	6.03	0.21	51.4	4.37	5.20	0.23	3.82	0.08
Zn	675	35.6	654	14.4	412	8.58	36.0	1.17	375	9.29	40.2	0.44	18.3	0.42	228	12.1	19.1	0.65	10.7	0.43
Ga	3.83	0.08	4.29	0.16	3.59	0.06	5.11	0.15	4.05	0.13	4.86	0.14	4.57	0.14	3.82	0.09	5.12	0.15	3.82	0.07
Rb	2.11	0.01	2.06	0.06	2.12	0.02	3.17	0.10	2.49	0.12	3.32	0.07	5.01	0.13	1.76	0.08	3.58	0.04	3.79	0.06
Sr	298	3.14	302	9.06	300	12.5	202	8.03	318	10.1	199	1.97	186	5.33	289	5.40	183	5.05	190	6.30
Y	111	1.83	115	4.03	128	2.99	59.0	1.36	140	3.86	60.1	1.05	61.6	0.97	105	2.08	52.5	0.64	96.3	2.86
Zr	312	0.56	294	5.73	358	10.1	224	4.10	328	8.12	221	6.18	312	5.48	254	3.90	243	8.86	237	3.07
Nb	21.4	0.27	21.5	0.92	22.3	0.13	19.8	0.56	24.6	0.76	16.6	0.18	19.0	0.49	21.0	0.38	16.3	0.36	25.2	0.76
Sb*	12.5	1.33	1111	65.9	383	146	260	61.7	827	141	907	51.8	348	42.3	59.2	12.9	948	130	84.7	26.4
Cs*	757	41.2	793	19.2	763	55.9	1524	69.6	1140	83.5	791	75.7	2201	55.6	823	62.3	1798	147	1529	28.5
Ba	191	0.62	196	4.27	197	3.64	165	0.87	224	6.32	153	1.16	197	5.42	187	3.54	168	4.00	170	3.95
La	14.4	0.15	14.9	0.14	14.5	0.08	15.2	0.23	16.5	0.60	14.4	0.12	19.7	0.23	12.7	0.21	16.2	0.45	28.8	0.56
Ce	44.8	0.85	43.0	2.07	44.0	0.34	41.7	0.63	48.6	0.40	41.1	0.63	52.9	1.28	41.0	0.87	43.0	0.70	80.8	0.83
Pr	6.62	0.07	6.77	0.17	6.56	0.13	5.64	0.08	7.61	0.25	5.71	0.14	6.95	0.11	6.36	0.06	5.72	0.02	10.7	0.19
Nd	36.9	0.60	37.3	0.64	35.9	1.25	27.6	0.40	41.4	0.91	28.5	0.93	32.8	1.05	35.5	1.52	27.3	1.32	50.4	0.79
Sm	13.3	0.28	13.6	0.51	13.1	0.19	8.41	0.23	14.8	0.79	9.02	0.30	9.59	0.52	13.2	0.28	7.86	0.17	14.0	0.33
Eu	2.64	0.01	2.68	0.04	2.59	0.04	1.50	0.06	2.91	0.05	1.58	0.02	1.36	0.03	2.69	0.07	1.31	0.05	1.37	0.06
Gd	18.4	0.37	18.3	0.44	19.5	0.36	11.3	0.06	18.9	0.46	12.5	0.10	11.8	0.43	20.6	0.61	10.6	0.38	18.8	0.77
Tb	2.95	0.08	3.26	0.09	3.06	0.10	1.76	0.04	3.43	0.01	1.85	0.03	1.84	0.08	3.10	0.11	1.51	0.07	2.80	0.06
Dy	21.0	0.23	22.7	0.50	21.4	0.55	12.1	0.19	23.6	0.66	12.9	0.15	12.6	0.34	21.0	0.54	10.7	0.23	18.6	0.28
Ho	4.43	0.07	4.74	0.17	4.25	0.10	2.43	0.07	4.73	0.05	2.63	0.07	2.51	0.05	4.21	0.01	2.06	0.05	3.68	0.08
Er	12.8	0.19	13.9	0.21	12.5	0.27	7.07	0.06	13.9	0.60	7.66	0.09	7.34	0.18	12.7	0.51	6.23	0.30	10.6	0.21
Tm	1.80	0.03	1.95	0.06	1.80	0.03	1.00	0.02	1.98	0.02	1.09	0.02	1.04	0.03	1.79	0.05	0.87	0.03	1.50	0.03
Yb	11.7	0.04	13.2	0.36	11.7	0.54	6.59	0.07	13.0	0.08	7.01	0.23	6.50	0.22	11.7	0.25	5.61	0.23	9.44	0.23
Lu	1.67	0.01	1.87	0.04	1.68	0.07	0.92	0.02	1.88	0.05	1.00	0.04	0.92	0.02	1.78	0.03	0.83	0.06	1.30	0.02
Hf	9.47	0.19	10.1	0.38	9.67	0.31	6.23	0.09	10.6	0.21	6.78	0.15	7.04	0.26	9.06	0.21	5.74	0.21	5.99	0.09
Ta	1.21	0.01	1.07	0.02	1.17	0.02	0.78	0.04	1.20	0.05	1.01	0.08	0.91	0.06	1.27	0.06	0.73	0.02	1.16	0.06
Pb	0.97	0.03	0.94	0.05	0.74	0.02	7.72	0.18	1.70	0.07	7.71	0.20	7.06	0.37	0.77	0.03	7.58	0.18	7.49	0.36
Th	1.75	0.06	1.89	0.04	1.77	0.04	2.35	0.06	2.07	0.04	2.22	0.09	3.33	0.08	1.53	0.07	2.69	0.03	4.47	0.09
U	0.45	0.02	0.51	0.00	0.45	0.00	0.61	0.01	1.51	0.02	0.60	0.02	0.81	0.05	0.41	0.02	1.02	0.04	0.95	0.01

WR subsamples are identified by lithologic type such that B-basalt, X-breccia, and M-mixture of basalt and breccia. Trace elements are listed in ppm except for elements denoted by *, which are listed in ppb. Elements that are below detection limit are denoted by n.d. Standard Deviations of ICP-MS data are shown in columns indicated by ±.

Table 7
Measured and certified trace element concentrations (ppm) of USGS Standard Reference Materials analyzed along with the 60639 whole-rock aliquots (Tables 5 and 6).

Standard Reference Material	BCR-2		BHVO-2		BIR-1		BHVO-1	
Avg. this study and certified values	Avg	Cert.	Avg	Cert.	Avg	[1]	Avg	Cert.
Li	8.79	9.00	7.94	5.00	3.24		5.33	4.60
Be	2.08		0.97		0.10		0.95	0.88
Sc	32.7	33.0	29.4	32.0	44.8	46.1	34.0	33.8
V	454	416	309	317	356	346	381	351
Cr	16.4	18.0	288	280	435		364	352
Co	37.1	37.0	42.1	45.0	55.3		50.6	54.0
Ni	11.7		115	119	187		144	133
Cu	20.6	19.0	124	127	132		158	183
Zn	143	188	117	103	78.7		176	105
Ga	21.9	23.0	20.1		16.6		24.5	23.8
Rb	48.5	48.0	9.74	9.80	0.19	0.17	9.63	9.86
Sr	348	346	429	389	121	112	413	407
Y	31.5	37.0	24.9	26.0	14.9	14.6	23.1	25.2
Zr	174	188	170	172	14.9	15.7	162	172
Nb	13.2		22.6	18.0	0.67	0.74	20.8	19.0
Sb[*]	0.30		0.19		0.52		0.18	0.17
Cs[*]	1.09	1.10	0.09		0.00		0.09	0.07
Ba	666	683	131	130	6.62	6.47	126	137
La	23.3	25.0	15.2	15.0	0.61	0.61	14.3	15.9
Ce	53.1	53.0	37.9	38.0	1.89	1.93	39.6	40.8
Pr	6.29	6.80	5.04		0.35	0.38	5.27	5.88
Nd	29.4	28.0	24.4	25.0	2.44	2.47	24.9	25.0
Sm	6.50	6.70	6.20	6.20	1.15	1.14	6.03	6.68
Eu	1.87	2.00	2.10		0.53	0.52	2.10	2.17
Gd	6.99	6.80	5.80	6.30	2.42	1.91	7.04	6.73
Tb	0.93	1.07	0.91	0.90	0.38	0.35	0.88	0.96
Dy	6.61		5.40		2.69	2.63	5.53	5.43
Ho	1.33	1.33	1.00	1.04	0.60	0.57	1.00	0.98
Er	3.81		2.65		1.78	1.72	2.55	2.57
Tm	0.49	0.54	0.33		0.27	0.26	0.33	0.34
Yb	3.35		2.02	2.00	1.66	1.71	2.03	2.00
Lu	0.50		0.28	0.28	0.27	0.26	0.29	0.28
Hf	4.97	4.80	4.70	4.10	0.58	0.64	4.70	4.45
Ta	0.75		1.16	1.40	0.12	0.21	1.10	1.15
Pb	9.81		2.65		3.03	3.13	2.01	2.13
Th	5.82	6.20	1.21	1.20	0.03	0.06	1.10	1.19
U	1.66	1.69	0.58		0.02	0.01	0.41	0.41

Trace elements are listed in ppm except for elements denoted by [*], which are listed in ppb. Standard deviations of ICP-MS data are shown in columns indicated by ±. Certified values for BIR-1 are from Xie et al. (1994). Certified values for other Standard Reference Materials are from the United States Geological Survey: http://crustal.usgs.gov/geochemical_reference_standards/.

of plagioclase → ilmenite → pyroxene (Delano, 1975). Among the pyroxenes analyzed for trace elements, the two most iron-rich are also the most enriched in the REE, reflecting the evolution of the melt. Whereas the 60639 basaltic pyroxenes contain up to 30 wt% FeO (Table EA1), the partition coefficients reported by Dygert et al. (2014) demonstrate that pyroxene partition coefficients change as composition varies.

Olivine compositions are similar to those reported by Delano (1975). Using the method of Delano (1980) for calculating the Fe–Mg K_D between olivine and liquid ($K_D = -0.0056 \times TiO_2 + 0.338$), it can be shown that the analyzed olivines are, for the most part, in equilibrium with the whole-rock. Using the whole-rock data in Table 6, equilibrium olivines should have composition of $Fo_{65.6}$ to $Fo_{70.2}$.

The analyzed olivines have a range of compositions from $Fo_{61.1}$ to $Fo_{70.6}$. The basaltic olivine crystals from 60639 have similar Fo contents and Co concentrations to Apollo 14 high-Al basalts, but higher Ti/V ratio than both Apollo 12 and 14 basalts (Fagan et al., 2013) suggesting that the basalt clasts may also be easily distinguished from basalts of other sites using the trace element contents of olivine. The 60639 basaltic olivine crystals are also distinct from samples from other Apollo missions, as they generally display a greater variation of Mn and Cr concentration than the Apollo 11 and 17 high-Ti basalts described in Shearer and Papike (2005). Yttrium and Mn behave incompatibly in basaltic olivine (Shearer and Papike, 2005), thus the olivine crystal with the highest Y and Mn concentrations (4.4 ppm and 2924 ppm, respectively) also has the highest
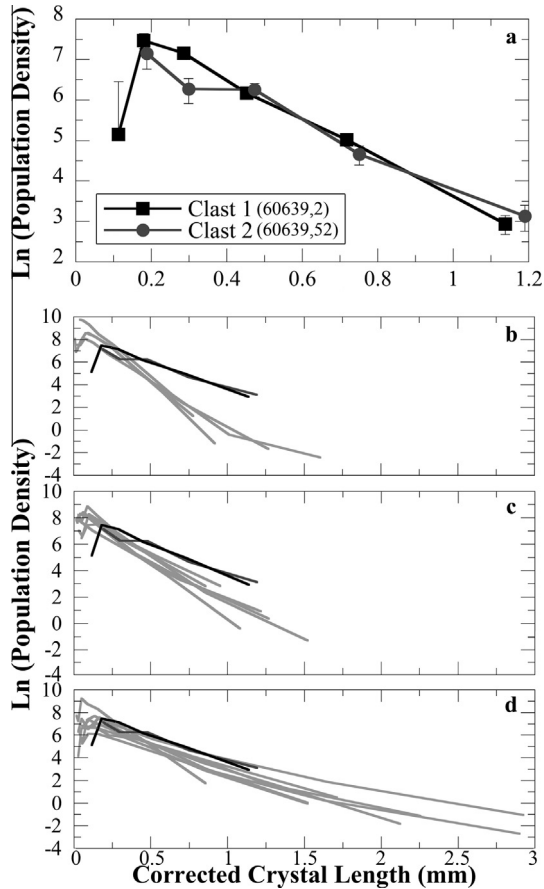
Fig. 8. CSD analyses are represented (a) as the corrected crystal length against the natural logarithm of the population density. Population density error bars are calculated from CSD Corrections and incorporate counting errors, errors in the shape probability parameters, and errors in the conversion of intermediate crystal dimensions or short crystal dimensions to crystal lengths (Higgins, 2000). Plagioclase CSDs from 60639 are compared to Apollo 14 high alumina basalt plagioclase CSDs (Hui et al., 2011) in (b)–(d). Basalts from Group A (b), Group B (c) and Group C (d) are defined by Neal and Kramer (2006). Note the different scales in (a) in contrast to (b)–(d).

Fig. 9. Selected 60639 basalt clast and breccia pyroxene major element concentrations that illustrate core-rim chemistry variations in Mg# and Cr_2O_3 (a) as well as the Ti/Al ratio (b). Pyroxene chemistry indicates a magma with increasing enrichment in Fe and decreasing enrichment in Ti and Al over time as the pyroxene rims become more Fe-rich (a) and depleted in Ti and Al (b).

Fe/(Fe+Mg), and is likely a late-stage crystal. In addition, this crystal has the lowest Ti concentration, suggesting that late-stage olivine crystallization may have continued after ilmenite came on the liquidus.

5.3. Whole-rock analyses

5.3.1. Basalt vs. breccia vs. mixed lithology

Analysis of the basalt, breccia and mixed lithology samples was conducted to determine if any of the basalt aliquots contained small portions of breccia matrix. It was expected that the mixed lithology subsamples from Clasts 2 and 3 would yield intermediate compositions between the breccia matrix and basalt. However, this is not the case (Fig. 7), as the mixed lithology subsamples do not lie on a simple two component mixing line for major and trace elements (Fig. 7a and b). The mixed lithology subsamples con-

tain similar Al_2O_3 concentrations as the breccia subsamples (Fig. 7a), and although they contain TiO_2 concentrations intermediate to the breccia and basalt samples, the Clast 2 mixed lithologies contain the lowest Hf contents of all samples (Fig. 7b). The Clast 3 mixed lithology subsample contains the lowest TiO_2 and Hf contents, forming an apparent end member in Fig. 7b.

The mixed-lithology subsamples therefore represent a conundrum, which is exemplified by the REE profiles (Fig. 7c). The breccia and mixed lithology subsamples display subparallel, LREE-enriched [$(La/Sm)_N > 1$], REE profiles (Fig. 7c). This signature contrasts with the profile of the basalt clasts that have $(La/Sm)_N < 1$. Surprisingly, the Clast 3 mixed lithology subsample, which is associated with the more REE-enriched breccia, is the least enriched of all the samples in nearly every REE (Fig. 7c). In addition to the REE, the mixed lithology subsamples are generally

similar to the breccias in most other trace elements (e.g., Sc, Co, Zn; Table 6).

The REE profiles of the mixed lithology samples indicate the influence of an additional component beyond the basalt and the analyzed breccia to account for their compositions. The breccia and mixed lithology REE profiles are the most distinct from the basalts in the LREE. The overall depletion of REE in the mixed lithology subsamples relative to the breccia matrix can be explained by the incorporation of varying amounts of plagioclase into an amalgamation of the average 60639 basalt component and the average of the two separate breccia matrix components from Clasts 2 and 3. A plagioclase composition from an Apollo 16 cataclastic anorthosite (60618,4; Fagan, 2012) is selected as a typical highlands plagioclase with most chondrite-normalized

REE concentrations of 6 or less, a large positive Eu anomaly, and An$_{97}$. By combining ~20% average 60639 basalt + 56% average Clast 2 breccia + 24% plagioclase, the calculated REE profile is a near perfect match to the average mixed lithology (Table 8). Likewise, a calculated combination of ~20% average 60639 basalt + 50% Clast 3 breccia + 30% plagioclase results in a similar calculated mixed lithology; the calculated mixture using the Clast 2 breccia is a closer match to the mixed lithology subsamples in both major and trace elements. The incorporation of highlands plagioclase increases the concentrations of plagiophile elements (i.e., Al$_2$O$_3$, CaO), which can explain the major and trace element compositions of the mixed lithology subsamples forming an apparent end member composition. The mixed lithologies that contain lower trace element con-

Table 8
60639 whole-rock mixing calculations.

	End-members				Measured mixture$_{avg}$	Calculated mixtures	
	Basalt$_{avg}$	Clast 2 X$_{avg}$	Clast 3 X$_{avg}$	Plagioclase $_{60335,13}$		20% B$_{avg}$ + 56% Clast 2 X + 24% Plag$_{60618}$	20% B$_{avg}$ + 50% Clast 3 X + 30% Plag$_{60618}$
Major and Minor element oxide concentrations (wt%)							
SiO$_2$	41.2[**]	48.2[**]	43.3[**]	43.6	44.2[**]	45.6	42.8
TiO$_2$	7.64	0.67	1.03	0.02	1.97	1.91	2.05
Al$_2$O$_3$	12.1	24.2	27.0	35.7	24.5	24.6	26.6
Cr$_2$O$_3$	0.26	0.11	0.10	0.01	0.12	0.12	0.10
FeO	18.7	5.43	5.73	0.18	7.29	6.82	6.66
MnO	0.26	0.06	0.07	0.02	0.10	0.09	0.09
MgO	7.82	6.64	6.03	0.05	6.35	5.29	4.59
CaO	11.3	13.9	16.1	19.6	14.9	14.8	16.2
Na$_2$O	0.52	0.48	0.43	0.39	0.46	0.47	0.44
K$_2$O	0.16	0.22	0.15	0.00	0.16	0.16	0.11
P$_2$O$_5$	0.18	0.30	0.32	N.A.	0.20	0.20	0.20
Trace element concentrations (ppm)							
Sc	64.3	9.55	9.98	22.9	12.4	23.7	24.7
Cr	2026	754	577	6.82	891	829	696
Sr	299	186	190	170	195	205	206
Y	118	61.6	96.2	1.35	57.2	58.4	72.1
Zr	309	312	237	52.1	229	249	196
La	14.3	19.7	28.8	1.35	15.2	14.2	17.7
Ce	43.9	52.9	80.8	2.42	41.9	39.0	49.9
Pr	6.68	6.95	10.7	0.29	5.69	5.30	6.77
Nd	36.9	32.8	50.2	1.03	27.8	26.0	32.8
Sm	13.4	9.59	14.1	<0.19	8.43		
Eu	2.68	1.36	1.37	0.59	1.47	1.44	1.40
Gd	19.3	11.8	18.1	0.27	11.5	10.5	13.0
Tb	3.12	1.84	2.80	<0.03	1.71		
Dy	21.6	12.6	18.6	0.14	11.9	11.4	13.7
Ho	4.41	2.51	3.68	0.03	2.37	2.30	2.73
Er	12.9	7.34	10.6	0.10	6.99	6.71	7.91
Tm	1.84	1.04	1.50	<0.02	0.99		
Yb	12.1	6.50	9.44	0.11	6.41	6.09	7.17
Lu	1.75	0.92	1.30	0.03	0.92	0.87	1.01
Hf	9.64	7.04	5.99	1.03	6.25	6.12	5.23
Ta	1.20	0.91	1.16	0.05	0.84	0.76	0.83
Th	1.76	3.33	4.47	0.21	2.42	2.27	2.65
Eu/Eu*	0.50	0.39	0.26	>7.97	0.45	0.48	0.38

WR subsamples are identified by lithologic type such that B-basalt, X-breccia, and M-mixture of basalt and breccia. N.A. indicates that element was not analyzed. [**]Indicates SiO$_2$ calculated by difference. Eu/Eu* = Eu$_N$/[(Sm$_N$ + Gd$_N$)/2] and represents the relative magnitude of the Eu anomaly for the sample. 'N': chondrite-normalized value. Eu/Eu* values for the calculated mixtures are only an approximation, as they do not consider Sm values because the Sm concentration of the plagioclase is below the detection limit.

tents than the breccia samples, yet have subparallel REE profiles to them, can be explained by a simple incorporation of excess plagioclase (which is a dominant phase at the Apollo 16 highlands site) as a third mixing component, thus diluting the breccia matrix composition; this incorporation likely occurred via impact mixing. We can conclude that the basalt aliquots were indeed pure basalt and did not contain any adhering breccia matrix.

5.3.2. Compositions of 60639 basalt

Previous studies have reported petrographic, mineral, and whole-rock data from a single 60639 basalt clast (,1) and noted similarities with basalts from Luna and other Apollo missions (Dowty et al., 1974; Delano, 1975; Murali et al., 1976). Dowty et al. (1974) suggested a similarity in composition to Luna 16 ilmenite-rich basalts (e.g., Keil et al., 1972) and thus a possible origin from Mare Fecunditatis, although they acknowledge that the nearest high-Ti mare source is Nectaris. The results from this work show that the 60639 basalt clasts have TiO_2 concentrations (7.4–7.9 wt%) that correlate with orbital data for Nectaris, but the FeO concentrations (17.8–19.4 wt%) are ~3–5 wt% higher than that detected from orbit (Lucey et al., 1998; Elphic et al., 2002; Gillis et al., 2006). Murali et al. (1976) published compositions of two subsamples from Clast 1 and suggested that the titaniferous basalt was similar in composition to the low alkali Apollo 11 and 17 mare basalts, but with slightly lower TiO_2. Ma et al. (1976) noted a linear correlation between Apollo 11 (low and high alkali variants) high-Ti mare basalts for La vs. La/Sm and La vs. Sm/Eu and suggested a common genetic link; the 60639 basalt clast reported by Murali et al. (1976) falls on the Apollo 17 trend on a plot of La vs. Sm/Eu (Fig. 7a of Ma et al., 1976) but falls between the Apollo 11 low- and high-K, high-Ti basalts (Fig. 7b of Ma et al., 1976). The whole-rock compositions from this study also lie on the Apollo 11 and Apollo 17 high-Ti basalts trends of Ma et al. (1976), and as expected, the breccia and mixed lithology subsamples distinctly fall off this trend.

The combination of chemical and textural data for 60639 basalts (data reported here and earlier; Dowty et al., 1974; Delano, 1975; Murali et al., 1976) shows that they are generally distinct from other previously analyzed Apollo 16 basalts (Simon and Papike, 1987; Hughes and Schmitt, 1988; Zeigler et al., 2006; Neal et al., 2015), which is consistent with the conclusion that basalts from the Apollo 16 site likely represent ejecta from remote localities (Dowty et al., 1974; Zeigler et al., 2006). Zeigler et al. (2006) demonstrated the presence of basaltic samples similar in major element composition to various basalt types including Apollo 11 high-Ti, Apollo 14 high-Al, Apollo 17 very low-Ti (VLT), and Luna 24 VLT all at the Apollo 16 site. Of the samples examined by Zeigler et al. (2006), only one (60503,22–7) has similar TiO_2 (8.7 wt%) and FeO (18.4 wt%) to the 60639 basalt clasts reported here (Fig. 10b). However, the Al_2O_3 (9.9 wt%) and Na_2O (0.30 wt%) concentrations are lower in 60503,22–7 than the 60639 basalt clasts (in keeping with the plagioclase-rich nature of the latter; Fig. 10); in addition, the trace element chemistry and texture of 60503,22–7, which is a
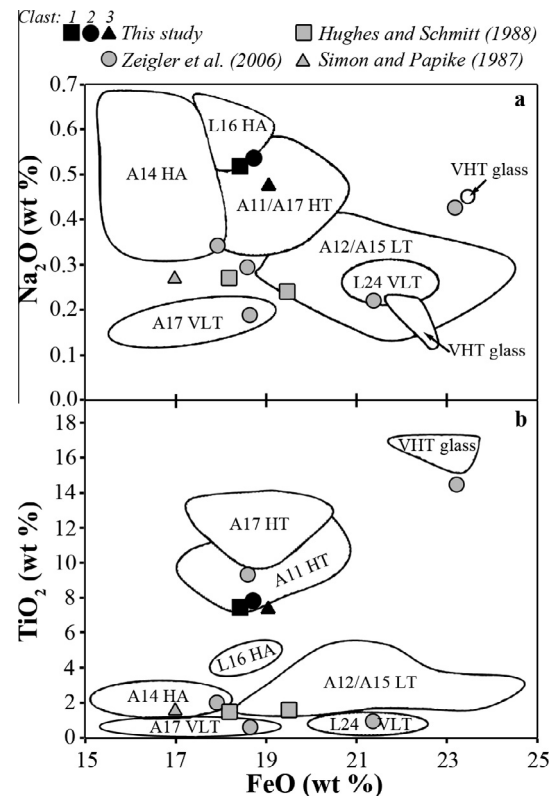

Fig. 10. 60639 whole-rock basalt clast major element compositions in comparison with other Apollo 16 basalts from Simon and Papike (1987), Hughes and Schmitt (1988), and Zeigler et al. (2006). Compositional basalt fields from other Apollo and Luna missions are also shown (modified from Zeigler et al., 2006). FeO concentrations (a and b) of the 60639 basalt clasts are similar to some Apollo 16 basalts from Hughes and Schmitt (1988) and Zeigler et al. (2006). Na_2O concentrations (a) of the 60639 basalt clasts are similar to Luna 16 high-Al basalts as well as Apollo 11 and Apollo 17 high-Ti basalts; TiO_2 concentrations (b) of the 60639 basalt clasts are similar to the Apollo 11 high-Ti basalts, but are lower than the Apollo 17 high-Ti basalts.

vitrophyric basalt, are dissimilar to the 60639 basalt clasts. Another clast examined by Zeigler et al. (2006), sample 60053,2–9, is a coarse-grained basalt with similar modes of pyroxene (50%), plagioclase (25%), and ilmenite (6%) to 60639 basalt clasts, but contains no olivine and has a distinct whole-rock composition. In contrast, sample 60603,10–16 (Zeigler et al., 2006), another vitrophyric basalt, contains similar concentrations of the REE, Zr (380 ppm), Hf (11.1 ppm), Ba (222 ppm), Th (1.6 ppm), and U (0.45 ppm) to the 60639 basalt clasts, but has much lower Al_2O_3 (5.5 wt%) and higher TiO_2 (14.5 wt%).

Although most major element data are similar to Apollo 11 and 17 high-Ti basalts (Fig. 10a and b), the 60639 basalt clasts do not fall consistently within any of the defined Apollo 11 high-Ti basalt groups described by Beaty et al. (1979) and Jerde et al. (1994) (Figs. 11 and 12). For example, the 60639 clasts appear to be similar to Apollo 11 Group B2 and Group D basalts in terms of Al_2O_3, TiO_2, Al/Ti, and Ca/Al (Fig. 11) and they are distinct from the Apollo 17 high-Ti basalts and the Apollo 12 ilmenite
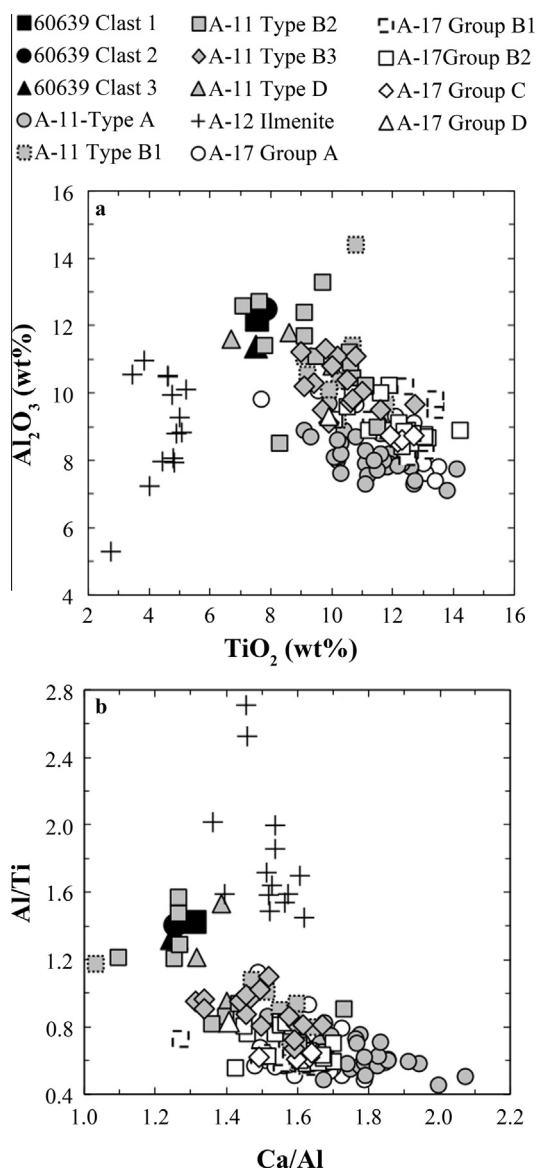
Fig. 11. Selected major element chemistry comparison between the average 60639 basalt clasts and high-Ti (HT) basalts from Apollo 11, 12, and 17. The TiO_2 concentration (a) of the 60639 basalt clasts is lower than most of the Apollo 11 and 17 HT basalts whereas the Al_2O_3 concentration is higher than most Apollo 11 and 17 HT basalts; however, the concentrations are similar to some Apollo 11 Type B2 and Type D basalts. The 60639 basalt clasts also have similar Al/Ti and Ca/Al ratios (b) to the Apollo 11 Type B2 and Type D basalts. Apollo 11, 12, and 17 data from the Mare Basalt Database and references therein (www3.nd.edu/~cneal/Lunar-L/Mare-Basalt-Database).

basalts. When the minor and trace elements are considered, a very different picture develops. The 60639 basalts are compositionally intermediate between the Apollo 11 Group A and the Group B1 basalts when plotting concentrations of K_2O vs. La and K_2O vs. Cr/La (Fig. 12).

The Sc/Sm ratio can be used to trace the effects of pyroxene fractionation (e.g., Norman and Ryder, 1980).

Significant pyroxene removal during crystal fractionation would drive the magma to lower Sc/Sm values. However, if pyroxene is retained in the source region the resultant magma would also have a low Sc/Sm ratio. The 60639 basalts exhibit relatively low Sc/Sm values (<6) and plot with the Apollo 11 Group A, B1 and B2 basalts in Fig. 12c and d. Critically though, the complete lack of pyroxene phenocrysts suggests the low Sc/Sm ratios are not due to crystal fractionation, but rather a relatively low degree of partial melting that retained some pyroxene in the mantle residue.

The role of ilmenite can be evaluated in Fig. 12d and e. Both La and Hf are incompatible in olivine, plagioclase, and pyroxene, so fractionation of these minerals should not change the La/Hf ratios. Ilmenite, however, has the potential to change this ratio, as Hf is less incompatible than the LREE by about two orders of magnitude (e.g., McKay et al., 1986; Nakamura et al., 1986). Therefore, crystal fractionation of ilmenite would increase the La/Hf ratio in a given basalt suite, whereas ilmenite accumulation would decrease this ratio. Many of the different high-Ti basalt suites exhibit a constant La/Hf ratio (Fig. 12d and e). The 60639 basalt clasts have an average La/Hf ratio of 1.48 ± 0.07 suggesting ilmenite fractionation did not dramatically affect these basalts, but there are only 3 samples from this group. In contrast, the three Apollo 11 Group D basalts have an average La/Hf ratio of 2.64 ± 0.11 suggesting ilmenite fractionation may have affected the Group D basalts and that the 60639 basalts were derived from a different source. The Apollo 11 Group A and B2 basalts also exhibit notable ranges in La/Hf, as do the Apollo 12 ilmenite basalts, which have been affected by crystal fractionation and accumulation (Neal et al., 1994).

The slope of the REE profile is sensitive to the degree of partial melting. In order to present a substantial amount of REE data from all high-Ti mare basalts, $(Ce/Sm)_N$ can be plotted against $(Ce/Yb)_N$ (Fig. 12f). That is, the slope of the light REE plotted against the slope of the entire REE profile, where both ratios are normalized to chondrites (Anders and Grevesse, 1989). Using these slopes, the 60639 basalts plot with the Apollo 11 Group B3 basalts and the Apollo 12 ilmenite basalts (Fig. 12f). The 60639 basalts have REE profiles that are slightly LREE-depleted (Figs. 7c and 12f) and are generally distinct from the Apollo 17 high-Ti basalts.

The textures of the 60639 basalts (Figs. 2 and 3) show little evidence for crystal fractionation (i.e., a lack of *bone fide* phenocrysts), indicating the whole-rock compositions can be used to infer source and melt generation characteristics. The whole-rock data suggest that the 60639 basalts were derived from an evolved source region (low Cr/La, Fig. 12b and c) through relatively moderate degrees of partial melting that produced slightly LREE-depleted REE profiles (Fig. 12f); low degrees of partial melting would yield $(Ce/Yb)_N$ and $(Ce/Sm)_N > 1$. The source region was enriched in K, REE, (Fig. 12a) and other incompatible trace elements and was probably rich in pyroxene, which was not exhausted upon partial melting resulting in low Sc/Sm ratios for the derived melt (Fig. 12c and d). As noted above,
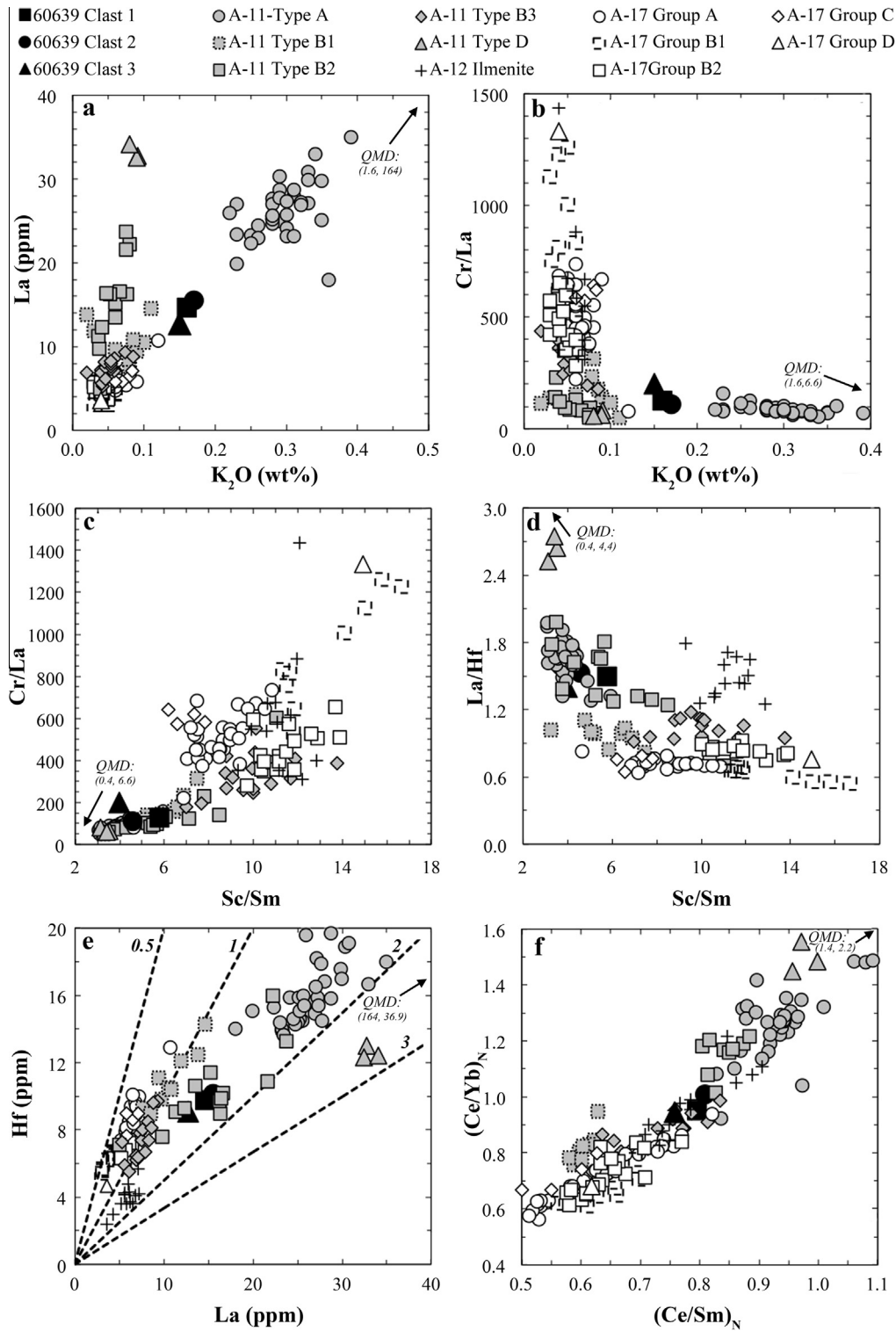
Fig. 12. Selected minor and trace element chemistry comparisons between the average 60639 basalt clasts and high-Ti (HT) basalts from Apollo 11, 12, and 17 (see Fig. 11). The 60639 basalt clasts appear to compositionally lie between the Apollo 11 Type A and Type B1 basalts considering K$_2$O and La concentrations (a; figure modified from Jerde et al.,1994) and (b). The 60639 basalt clasts have low Sc/Sm ratios (<6), which is similar to the Apollo 11 Type A, B1, and B2 basalts (c and d), and may reflect the extent of pyroxene fractionation. The influence of ilmenite is illustrated in (d) and (e), as ilmenite affects the La/Hf ratio. The slopes of the rare-earth element profiles are shown in (f), where (Ce/Yb)$_N$ represents the slope of the LREE and (Ce/Sm)$_N$ represents the slope of the entire REE profile where both ratios are normalized to chondrites (Anders and Grevesse, 1989). The average QMD composition (calculated from Marvin et al., 1991) is noted in each of the panels of Fig. 12a–f. Apollo 11, 12, and 17 data from the Mare Basalt Database and references therein (www3.nd.edu/~cneal/Lunar-L/Mare-Basalt-Database).

the lack of pyroxene phenocrysts in the 60639 basalts (Figs. 2 and 3) indicates crystal fractionation was not responsible for the low Sc/Sm values.

5.4. Petrogenesis of the 60639 basalts

The 60639 basalt clasts plot at the lower end of the high-Ti basalt designation (cf. Neal and Taylor, 1992), but they contain relatively high Al_2O_3 contents (Fig. 11a), similar to the Apollo 14 high-Al basalts (e.g., Neal and Kramer, 2006). In terms of Al_2O_3 and TiO_2 contents, the 60639 basalts are similar to the Group D basalts and some of the more fractionated Group B2 basalts from Apollo 11 (Beaty et al., 1979; Ma et al., 1980; Jerde et al., 1994) (Fig. 11a). However, the K_2O concentrations of the 60639 clasts are unique amongst the high-Ti basalts returned from the Moon (Fig. 12a and b). The 60639 clasts appear to have been derived from a fractionated source with low Cr/La concentrations similar to the Apollo 11 Group A basalts (Fig. 12b and c), but with different concentrations in other trace elements such as Hf, La, and the Sc/Sm ratio (Fig. 12d and e). In terms of the REE profiles, though, the 60639 basalts are distinct from Apollo 17 high-Ti basalts and are similar to some of the Apollo 11 Type B3 basalts (Fig. 12f).

The lack of consistent overarching similarities with another single high-Ti basalt group indicates that the 60639 basalts are a unique type of basalt that has not previously been recognized in the current sample collection. That being said, the 60639 basalts do have similar Cr/La, K/La, La/Hf and Sc/Sm ratios to the high-K Apollo 11 Group A basalts (Fig. 12a–e). Jerde et al. (1994) concluded that the Apollo 11 Group A basalts were derived from a source region that is distinct from the other Apollo 11 high-Ti basalt groups, and assimilated an evolved KREEP-like material that was much younger than urKREEP (cf. Warren, 1985). This component was coined "neu-KREEP" (Jerde et al., 1994) and was similar to the composition of quartz monzodiorite (QMD) described from the Apollo 15 site (e.g., Marvin et al., 1991). The average QMD composition (calculated from Marvin et al., 1991) is noted in each of the panels of Fig. 12a–f. The 60639 basalts lie on a trajectory between QMD and a parent approximated by the Apollo 11 Group B3 basalt (Fig. 12a–f). Note that Jerde et al. (1994) used an Apollo 11 orange glass composition as the parent for these basalts (composition from Delano, 1986) in their modeling. Qualitatively speaking, the Apollo 11 Group A basalts contain the highest QMD signature followed by the 60639 basalts. The Apollo 11 Group B1 basalts also appear to lie on this trajectory (Fig. 12a–e), but apparently experienced smaller degrees of assimilation of QMD compared to the 60639 and Group A basalts. Jerde et al. (1994) concluded that the Apollo 11 Group B1 basalts (along with groups B3 and D) were not affected by such assimilation; Fig. 12f supports this conclusion, as the B1 basalts are the most LREE-depleted of all the Apollo 11 basalt groups.

The implication from the discussion above is that the 60639 basalts also may have experienced evolution through assimilation of a QMD-like material. While the petrogenetic process may have been similar to that proposed for the Apollo 11 Group A basalts, the higher Al/Ti and lower Ca/Al ratios (Fig. 11b) of the 60639 basalts suggest derivation from a source unrelated to the Apollo 11 basalts. Another implication is that an evolved, QMD-like material was also present in the crust beneath the lava flows from which the 60639 basalt clasts were derived. Using the neu-KREEP composition (Jerde et al., 1994) and the measured Apollo 11 Orange glass composition (Shearer and Papike, 1993) as the parent composition, the REE profiles and K_2O content of the average Apollo 11 Type A basalt composition can be produced by bulk mixing of ~15% neu-KREEP with 85% of the parent. The REE profiles and K_2O content of 60639 basalts require ~7% of the neu-KREEP component. Few other trace elements are given for neu-KREEP by Jerde et al. (1994), hence we show the average composition of QMD from Marvin et al. (1991) in Fig. 12. Bulk mixing rather than assimilation coupled with fractional crystallization (AFC) is used because of the lack of phenocrysts in the 60639 basalts, and this process also approximates the Apollo 11 Type A basalts.

Neal and Taylor (1992) proposed a lunar mare basalt classification based primarily on TiO_2, with secondary and tertiary subdivisions based upon Al_2O_3 and K contents, respectively (see Fig. 3 in Neal and Taylor, 1992). The primary groups are very-low-Ti, low-Ti, and high-Ti with subdivisions placed at 1 and 6 wt% TiO_2, respectively. Each of these Ti groups was divided into high- and low-Al (division at 11 wt% Al_2O_3), and then each of these Ti-Al groups was subdivided into low- and high-K (division at 2000 ppm K). Therefore, Neal and Taylor (1992) proposed a 12-fold classification scheme for mare basalts, seven of which were populated by samples. The 60639 basalts are the first samples to fall within the proposed high-Ti/high-Al/low-K group.

6. SUMMARY AND CONCLUSIONS

Mineral compositions are indistinguishable between the 60639 basalt clasts indicating that the aliquots are derived either from a single basalt flow or from the same horizon of different flows of the same composition. The breccia matrix is derived from material other than the basalts as demonstrated by different mineral compositions.

Basalt + breccia matrix mixed lithology whole-rock analyses compositionally cluster together indicating similar end-member components, but the two breccia analyses are compositionally distinct from one another suggesting the breccia composition is variable. Such a mixture requires a third component, such as excess plagioclase. The trace element concentrations and REE profiles of the mixed lithology subsamples can be accounted for by mixing ~20% basalt + 61% Clast 2 breccia + 19% plagioclase or, similarly, ~20% basalt + 40% Clast 3 breccia + 40% plagioclase, where plagioclase acts as an analog for anorthosite.

These basalts evolved through ~7% assimilation of a QMD-like material. However, the textures show a lack of phenocrysts indicating that assimilation was not accompanied by fractional crystallization. The low Sc/Sm and Cr/La ratios exhibited by the 60639 basalts suggest derivation from an evolved, pyroxene-rich source region. We conclude

that the 60639 basalts represent the first example of a high-Ti/high-Al/low-K lunar basalt from the Moon. These basalts were derived from a source region enriched in ilmenite, plagioclase, and pyroxene (i.e., late-stage cumulates) and that pyroxene was retained in the mantle residue after melting; this is consistent with a shallow source, as the denser ilmenite will sink, but the lighter plagioclase will not, and the Sc/Sm ratio will be low. Although this could indicate that not all ilmenite sank during evolution of the Lunar Magma Ocean, such a conjecture is beyond the scope of this study. These basalts may have been derived from Mare Nectaris as the TiO_2 content seems to be consistent, although the FeO content of the 60639 basalts is higher than what appears to be defined for this area from remote sensing (17–19 wt% vs. 14–15 wt%).

ACKNOWLEDGEMENT

APPENDIX A. SUPPLEMENTARY DATA

Supplementary data associated with this article can be found, in the online version, at http://dx.doi.org/10.1016/j.gca.2015.08.007.

REFERENCES

Anders E. and Grevesse N. (1989) Abundances of the elements: meteoritic and solar. *Geochim. Cosmochim. Acta* **53**, 197–214.

Beaty D. W., Hill S. M. R. and Albee A. L. (1979) The petrology and chemistry of basaltic fragments from the Apollo 11 soil, part 1. *Proceed. Lunar Planet. Sci. Conf.* **10**, 41–75.

Cashman K. V. and Marsh B. D. (1988) Crystal size distribution (CSD) in rocks and the kinetics and dynamics of crystallization II: Makaopuhi lava lake. *Contrib. Mineral. Petrol.* **99**, 292–305.

Delano J. W. (1975) Petrology of the Apollo 16 mare component: Mare Nectaris. *6th Proc. Lunar Sci. Conf.*, 15–47.

Delano J. W. (1980) Chemistry and liquidus phase relations of Apollo 15 red glass: Implications for the deep lunar interior. *11th Proceed. Lunar Sci. Conf.*, 251–288.

Delano J. W. (1986) Pristine lunar glasses: Criteria, data, and implications. *16th Proceed. Lunar Sci. Conf.* **5**, D201–D213.

Dowty E., Keil K. and Prinz M. (1974) Igneous rocks from Apollo 16 rake samples. *5th Proceed. Lunar Sci. Conf.*, 431–445.

Dygert N., Liang Y., Sun C. and Hess P. C. (2014) An experimental study of trace element partitioning between augite and Fe-rich basalts. *Geochim. Cosmochim. Acta* **132**, 170–186.

Elphic R. C., Lawrence D. J., Feldman W. C., Barraclough B. L., Gasnault O. M., Maurice S., Lucey P. G., Blewett D. T. and Binder A. B. (2002) Lunar prospector neutron spectrometer constraints on TiO_2. *J. Geophys. Res.* **107**. http://dx.doi.org/10.1029/2000JE001460.

Fagan A. L. (2012) Volcanic and impact processes on Mars and the Moon. Unpub. Ph. D. dissertation, Univ. Notre Dame. 308 pp.

Fagan A. L., Neal C. R., Simonetti A., Donohue P. H. and O'Sullivan K. M. (2013) Distinguishing between Apollo 14 impact melt and pristine mare basalt samples by geochemical and textural analyses of olivine. *Geochim. Cosmochim. Acta* **106**, 429–445.

Flanagan F. J. (1984) Three USGS mafic rock reference samples, W-2, DNC-1, and BIR-1. *US Geol. Surv. Bull.* **1623**, 54.

Garrison, Jr., J. R. and Taylor L. A. (1980) Genesis of highland basalt breccias: a view from 66095. *Proceed. Conf. Lunar Highlands Crust*, 395–417.

Gillis-Davis J. J., Lucey P. G. and Hawke B. R. (2006) Testing the relation between UV-vis color and TiO_2 content of the lunar maria. *Geochim. Cosmochim. Acta* **70**, 6079–6102.

Gladney E. S. and Roelandts I. (1988) 1987 compilation of elemental concentration data for USGS BIR-1, DNC-1, and W-2. *Geostand. Newslett.* **12**, 63–118.

Govindaraju K. (1994) 1994 compilation of working values and descriptions for 383 geostandards. *Geostand. Newslett.* **118**, 1–158.

Higgins M. D. (1996) Crystal size distributions and other quantitative textural measurements in lavas and tuff from Egmont volcano (Mt. Taranaki) New Zealand. *Bull. Volcanol.* **58**, 194–204.

Higgins M. D. (2000) Measurement of crystal size distributions. *Am. Mineral.* **85**, 1105–1116.

Higgins M. D. (2002) Closure in crystal size distributions (CSD), verification of CSD calculations, and the significance of CSD fans. *Am. Mineral.* **87**, 171–175.

Higgins M. D. and Chandrasekharam D. (2007) Nature of subvolcanic Magma Chambers, Deccan Province, India: evidence from quantitative textural analysis of plagioclase megacrysts in the giant plagioclase basalts. *J. Petrol.* **48**, 885–900.

Hinners N. W. (1972) Apollo 16 site selection. In *Apollo 16 Preliminary Science Report*, NASA, Washington, DC.

Hughes S. S. and Schmitt R. A. (1988) Chemistry of a unique low-titanium basalt clast extracted from 60255 regolith breccia. *19th Lunar Planet Sci. Conf.*, 515–516.

Hui H., Oshrin J. G. and Neal C. R. (2011) Investigation into the petrogenesis of Apollo 14 high-Al basaltic melts through crystal stratigraphy of plagioclase. *Geochim. Cosmochim. Acta* **75**, 6439–6460.

Jerde E. A., Snyder G. A., Taylor L. A., Liu Y.-G. and Schmitt R. A. (1994) The origin and evolution of lunar high-Ti basalts: Periodic melting of a single source at Mare Tranquilitatis. *Geochim. Cosmochim. Acta* **58**, 515–527.

Keil K., Kurat G., Prinz M. and Green J. (1972) Lithic fragments, glasses and chondrules from Luna 16 fines. *Earth Planet Sci. Lett.* **13**, 243–256.

Lindsley D. H., Papike J. J. and Bence A. E. (1972) Pyroxferroite: breakdown at low-pressure and high temperature (abstract). *In Lunar Sci. III*, 483–485.

Lucey P. G., Blewett D. T. and Hawke B. R. (1998) Mapping the FeO and TiO_2 content of the lunar surface with multispectral imagery. *J. Geophys. Res.* **103**, 3679–3699.

Ma M.-S., Murali A. V. and Schmitt R. A. (1976) Chemical constraints for mare basalt genesis. *7th Proceed. Lunar. Sci. Conf.*, 1673–1695.

Ma M.-S., Schmitt R. A., Beaty D. W. and Albee A. L. (1980) The petrology and chemistry of basaltic fragments from the Apollo 11 soil: Drive tubes 10004 and 10005. *11th Proceed. Lunar Planet Sci. Conf.*, 37–47.

Mahoney J. J., Fitton J. G., Wallace P. J., and Coffin M. (2001) Basement drilling of the Ontong Java Plateau: covering Leg 192 of the cruises of the Drilling Vessel "Joides Resolution", Apra Harbour, Guam, to Apra Harbor, Guam, Sites 1183–1187, 8 September-7 November 2000. In *Proc. Of the Ocean Drilling Program, Initial Reports*, 192. College Station, TX, USA, Texas A & M University Ocean Drilling Program. pp. 75.

Marsh B. D. (1988) Crystal size distribution (CSD) in rocks and the kinetics and dynamics of crystallization I. Theory. *Contrib. Mineral. Petrol.* **99**, 277–291.

Marsh B. D. (1998) On the interpretation of crystal size distributions in magmatic systems. *J. Petrol.* **39**, 553–599.

Marvin U. B., Lidstom M. M., Holmberg B. B. and Martinez R. R. (1991) New observations on the quartz Monzodiorite-Granite suite. *Proceed. Lunar Planet. Sci. Conf.* **21**, 119–135.

McKay G., Wagstaff J. and Yang S.-R. (1986) Zirconium, Hafnium, and Rare Earth Element partition coefficients for ilmenite and other minerals in high-Ti lunar mare basalts: an experimental study. *Proceed. Lunar Planet. Sci. Conf. 16, J. Geophys. Res.* **91**, D229–D237.

Morgan D. J. and Jerram D. A. (2006) On estimating crystal shape for crystal size distribution analysis. *J. Volcanol. Geotherm. Res.* **154**, 1–7.

Morris R. V., See T. H. and Horz F. (1986) Composition of the Cayley Formation at Apollo as inferred from impact melt splashes. *17th Proceed. Lunar Planet. Sci. Conf., J. Geophys. Res.* **90**, E21–E42.

Murali A. V., Ma M.-S. and Schmitt R. A. (1976) Mare basalt 60639, Another Eastern Lunar Basalt. *Lunar Planet. Sci. VII.*, 583–584.

Nakamura Y., Fujimaki H., Nakamura N., Tatsumoto M., McKay G. A. and Wagstaff J. (1986) Hf, Zr, and REE partition coefficients between ilmenite and liquid: implications for lunar petrogenesis. *Proc. Lunar Planet. Sci. Conf. 16, in J. Geophys. Res.* **91**, D239–D250.

National Research Council (2007) The scientific context for exploration of the Moon, final report. The National Academies Press, Washington, DC.

Neal C. R. (2001) Interior of the Moon: the presence of garnet in the primitive deep lunar mantle. *J. Geophys. Res.* **106**, 27865–27885.

Neal C. R. and Kramer G. Y. (2006) The petrogenesis of the Apollo 14 high-Al mare basalts. *Am. Mineral.* **91**, 1521–1535.

Neal C. R. and Taylor L. A. (1992) Petrogenesis of mare basalts: a record of lunar volcanism. *Geochim. Cosmochim. Acta* **56**, 2177–2211.

Neal C. R., Hacker M. D., Taylor L. A., Schmitt R. A. and Liu Y.-G. (1994) Basalt generation at the Apollo 12 site, part 2: source heterogeneity, multiple melts, and crustal contamination. *Meteoritics* **29**, 349–361.

Neal C. R., Donohue P. H., Fagan A. L., O'Sullivan K., Oshrin J. and Roberts S. (2015) Distinguishing between basalts produced by endogenic volcanism and impact processes: a non-destructive method using quantitative petrography of lunar basaltic samples. *Geochim. Cosmochim. Acta* **148**, 62–80.

Norman M. and Ryder G. (1980) Geochemical constraints on the igneous evolution of the lunar crust. *11th Proceed. Lunar Planet. Sci. Conf.*, 317–331.

Papike J. J., Hodges F. N. and Bence A. E. (1976) Mare basalts: crystal chemistry, mineralogy, and petrology. *Rev. Geophys. Space Phys.* **14**, 475–540.

Pearce N. J. G., Perkins W. T., Westgate J. A., Gorton M. P., Jackson S. E., Neal C. R. and Chenery S. P. (1997) A compilation of new and published major and trace element data for NIST SRM 610 and NIST SRM 612 glass reference materials. *Geostandard. Newslett.* **21**, 115–144.

Ryder G. and Norman M. (1980) Catalog of Apollo 16 Rocks. *NASA Cur. Branch Pub* **16904**, 52, JSC.

Shearer C. K. and Papike J. J. (1993) Basaltic magmatism on the Moon: a perspective from volcanic picritic glass beads. *Geochim. Cosmochim. Acta* **57**, 4785–4812.

Shearer C. K. and Papike J. J. (2005) Early crustal building processes on the Moon: models for the petrogenesis of the magnesian suite. *Geochim. Cosmochim. Acta* **69**, 3445–3461.

Simon S. B. and Papike J. J. (1987) Petrology of a low-titanium mare basalt from Apollo 16 regolith breccia 60255. *18th Lunar Planet. Sci. Conf.*, 922–923.

Sutton R. L. (1981) Documentation of Apollo 16 samples. In *Geology of the Apollo 16 area, central lunar highlands.* (Ulrich et al.) USGS Prof. Paper 1048.

Van Achterbergh E., Ryan C. G., Jackson S. E. and Griffin W. L. (2001) Data reduction software for LA-ICP-MS. In *Laser-Ablation-ICPMS in the Earth Sciences: Principles and Applications* (ed. P. Sylvester). Mineralogical Association of Canada, pp. 239–243.

Warren P. H. (1985) The magma ocean concept and lunar evolution. *Ann. Rev. Earth Planet. Sci.* **13**, 201–240.

Warren P. H. and Wasson J. T. (1978) Compositional-petrographic investigation of pristine nonmare rocks. *9th Proceed. Lunar Planet. Sci. Conf.*, 185–217.

Xie Q., Jain J., Sun M., Kerrich R. and Fan J. (1994) ICP-MS analysis of basalt BIR-1 for trace elements. *Geostand. Newslett.* **18**, 53–63.

Zeigler R., Korotev R. L., Haskin L. A., Jolliff B. L. and Gillis J. J. (2006) Petrography and geochemistry of five new Apollo16 mare basalts and evidence for post-basin deposition of basaltic material at the site. *Meteorit. Planet. Sci.* **41**, 263–284.

Associate editor: Maud Boyet